Evolution of the southwest Pacific across the last glacial cycle: Insights from a multi-proxy approach of biological export production

Master's Thesis

Faculty of Science

University of Bern

presented by

Benjamin Meier

2015

Supervisor:

Prof. Dr. Samuel L. Jaccard
Institute of Geological Sciences and Oeschger Centre for Climate Change Research

Co-Supervisor:

Dr. Jörg Lippold
Institute of Geological Sciences and Oeschger Centre for Climate Change Research

Abstract

Many studies have inferred a dominant role for the Southern Ocean in modulating glacial-interglacial variability of atmospheric pCO_2 [*Sigman and Boyle*, 2000]. The potential importance of the Southern Ocean for pCO_2 reflects its leverage on the efficiency of the global soft-tissue cycle, by which the photosynthetic production, sinking and remineralization of organic matter stores carbon in the ocean interior, thereby lowering atmospheric pCO_2. By reconstructing paleofluxes of export production and redox conditions at the sediment-water interface, inferences of past ocean dynamics can be made. Thus far, cores from the Atlantic sector of the Southern Ocean dominate available high-resolution sediment records. Here, new results from a sedimentary archive collected from the abyssal southwest Pacific at the location of today's Antarctic polar front are reported. In particular, multi-proxy ^{230}Th-normalized fluxes of export production and redox-sensitive trace metal records, covering the last glacial cycle, are presented. The records show a strong climate-related signal, with higher export fluxes during interglacials and lower values during cold stages, consistent with previously reported evidence from the South Atlantic and the SE Pacific signaling lower upward supply of subsurface nutrient-rich water masses. The data therefore provide the opportunity to compare past atmospheric pCO_2-changes with a well dated sub-millennially resolved record over a full glacial cycle from a region previously sparsely considered.

1. List of figures

2. Introduction

Global climate and atmospheric carbon dioxide concentrations (pCO_{2atm}) have been shown to hold a remarkably high correlation during the last 800,000 years (see Fig.1) [*Sigman et al.*, 2010]. Due to anthropogenic perturbation of the carbon cycle, mainly from burning fossil fuels and deforestation, current pCO_{2atm} is around 400 ppmv [*Dlugokencky and Tans*, 2015] and therefore higher than during this time period [*Lüthi et al.*, 2008]. The relation between global climate and pCO_{2atm} highlights the need for a coherent understanding of the carbon cycle to allow better predicting its future evolution. Besides direct anthropogenic input of CO_2, important changes in the fluxes and storage of carbon associated with climate change emerge. These long-term feedback processes can be inferred by studying the connection between climate and pCO_{2atm} in the past at times anthropogenic perturbations were inexistent. Paleoclimatological research has shown that the interwoven interactions between ocean physics and biology in particular in the Southern Ocean (SO) are key in modulating natural pCO_{2atm}-variations [*Hain et al.*, 2014].

In this chapter the fundamental mechanisms and characteristics of cold (glacial) and warm periods (interglacial) will be discussed, with a focus on the ocean's role in driving and amplifying past climate variability. Secondly, the far-reaching influence that SO's biology and circulation imposes on the global climate and carbon cycle will be outlined. Further on, the approach of this master thesis is explained and research questions specified.

2.1. Ice age, orbital variations and the carbon cycle

Advancing and retreating ice sheets have been identified almost two centuries ago [*Raymo and Huybers*, 2008]. The Quaternary Period, that is the last 2.6 million years, was characterized by multiple climatic oscillations. Ice ages were characterized by extensive northern hemisphere (NH) ice sheets covering large parts of North America, northern Europe and Greenland (still present), as well as extensive glaciations in mountain ranges including the Alps, and an expansion of the Antarctic ice sheets [*Broecker and Denton*, 1990]. According to environmental archives and ice sheet modeling a distinct drop in global sea level of about 120 meters compared to today was a direct consequence of ice accumulation on land during glacial maxima [*Fairbanks*, 1989; *Clark and Mix*, 2002]. Global temperatures were 3-4 °C cooler during the last glacial maximum (LGM) with large regional variability [*Shakun et al.*, 2012].

Marine sediment cores have provided evidence of a quasi-stationary cyclicity of natural Quaternary climate variability, calling for a comprehensive explanation of common mechanisms responsible for these variations [*Hays et al.*, 1976]. Already in the middle of the 19th century, the link between global climate and the spatial distribution of incoming solar radiation has been proposed [*Raymo and Huybers*, 2008]. Since the earth's orbit around the sun is not constant, the spatial and seasonal insolation varies along with the orbital parameters eccentricity, obliquity and precession. Eccentricity defines the changes in the shape of the orbital ellipsoid with a characteristically time period of 100 kiloyears (kyr), obliquity relates to the variation in earth's tilt with a period of 41 kyr, and precessional changes describe the wobbling of earth's axis with a period of 21 kyr [*Berger*, 1988]. Combining the variation in the three parameters results in cycling insolation changes, named "Milankovitch-cycles" after

astronomer Milutin Milankovitch [*Sigman and Boyle*, 2000].

Insolation changes related to eccentricity variations are relatively weak; however, it is the only parameter that affects the total incoming solar radiation [*Hays et al.*, 1976]. Obliquity modulates the magnitude of seasonality. A strong (weak) tilt of the earth's axis causes a more (less) pronounced seasonal temperature contrast on both hemispheres (in phase changes), respectively. On the other hand, precession causes antiphased changes between NH and SH, by determining the day during which the earth is closest to the sun (perihelion) and thus affects the duration and intensity of a particular season [*Berger*, 1988]. If precession dictates perihelion to occur in NH summer, then the day farthest away from the sun (aphelion) will be in NH winter. These conditions cause a more pronounced seasonality in the NH and a weaker seasonality in the SH, as austral summer then occurs during aphelion and austral winter coincides with perihelion. If eccentricity is largest, then precessional changes produce the largest degree of change in seasonal insolation [*Broecker and Denton*, 1990]. Hence, a minimum in NH summer insolation is found when obliquity is weak and precession dictates aphelion to occur during NH summer [*Raymo and Huybers*, 2008], conditions that will favor the development of large, regional ice-sheets.

As mentioned above, evidence based on marine sediment cores has revealed regular climate cyclicity in the past (Fig. 1). *Hays et al.* [1976] analyzed oxygen isotope ratios ($^{18}O/^{16}O$) in foraminiferal calcite, which are known to vary with the global volume of continental ice sheets, since the lighter isotope ^{16}O is preferentially evaporated and stored in ice. The $\delta^{18}O$-signal[1] of water molecules is incorporated into calcium carbonate ($CaCO_3$) shells of foraminifera, a surface-dwelling marine organism, providing the opportunity to infer $\delta^{18}O$ variations and consequently volumetric ice sheet changes in the past. Spectral analysis of $\delta^{18}O$ revealed distinct frequency peaks coincident with the aforementioned orbital parameters [*Hays et al.*, 1976; *Lisiecki and Raymo*, 2005]. The longest and most pronounced cycles in $\delta^{18}O$ were identified to show a periodicity of approximately 100 kyr similar to the eccentricity period, with a gradual cooling towards a glacial maximum followed by a rapid warming into an interglacial climate state. This was insofar surprising, as eccentricity has the weakest influence on insolation changes, which is why non-linear behavior of the climate system has been inferred [*Imbrie et al.*, 1993]. Examples of such non-linear responses that could generate the 100 kyr signal include ice sheet inertia and albedo feedback [*Clark*, 1999], as well as changes in the global carbon cycle [*Shackleton*, 2000]. The amplitude of solar forcing alone would be too small to explain the dramatic climatic changes, especially the rapid transitions and asymmetry of the climate cycles (Fig. 1) [*Sigman and Boyle*, 2000]. Thus, additional processes internal to the climate system must be considered.

Greenhouse gases and CO_2 in particular, are thought to be a possible modulator to translate gradual and regional orbital changes into more abrupt and global climate changes [*Shackleton*, 2000; *Sigman and Boyle*, 2000]. In the context of glacial-interglacial climate cycles, variable pCO_{2atm} affected the Earth's radiation balance through an amplifying positive feedback mechanism [*Sigman et al.*, 2010]. Early ice core results revealed a strong link between climate and pCO_{2atm}. During the last ice age, substantially lower pCO_{2atm}

[1] Oxygen isotope ratio: $\delta^{18}O = \left(\frac{\left(\frac{^{18}O}{^{16}O}\right)_{sample}}{\left(\frac{^{18}O}{^{16}O}\right)_{standard}} - 1 \right) * 1000‰$

concentrations were measured in ice-trapped air bubbles [*Neftel et al.*, 1982]. Later on, ice core records were extended back to 800,000 years before present (BP) covering the last eight glacial cycles. The remarkably high correlation between pCO_{2atm} and climate was registered over the entire time period, with higher pCO_{2atm} approaching 280 ppmv during interglacials, whereas lower pCO_{2atm} of about 180 ppmv were inferred for glacial stages (Fig. 1) [*Siegenthaler et al.*, 2005; *Lüthi et al.*, 2008]. The 100 ppmv change in pCO_{2atm} may account for a significant part of the temperature difference between the last ice age and the Holocene [*Petit et al.*, 1999; *Sigman and Boyle*, 2000]. A second important outcome from ice cores has been deuterium-based temperature reconstructions, from deuterium to hydrogen ratio with less deuterium indicating colder temperatures. These observations have revealed that pCO_{2atm} varied in concert with Antarctic temperature throughout the last deglaciation [*Monnin et al.*, 2001] and the last four glacial cycles [*Petit et al.*, 1999; *Siegenthaler et al.*, 2005]. Even though the rise of pCO_{2atm} lagged Antarctic warming during deglaciations, it lead the global temperature increase on decadal to centennial timescales, supporting the notion that pCO_{2atm} was an important, if not crucial component of ice age cycles [*Clark et al.*, 2009; *Shakun et al.*, 2012].

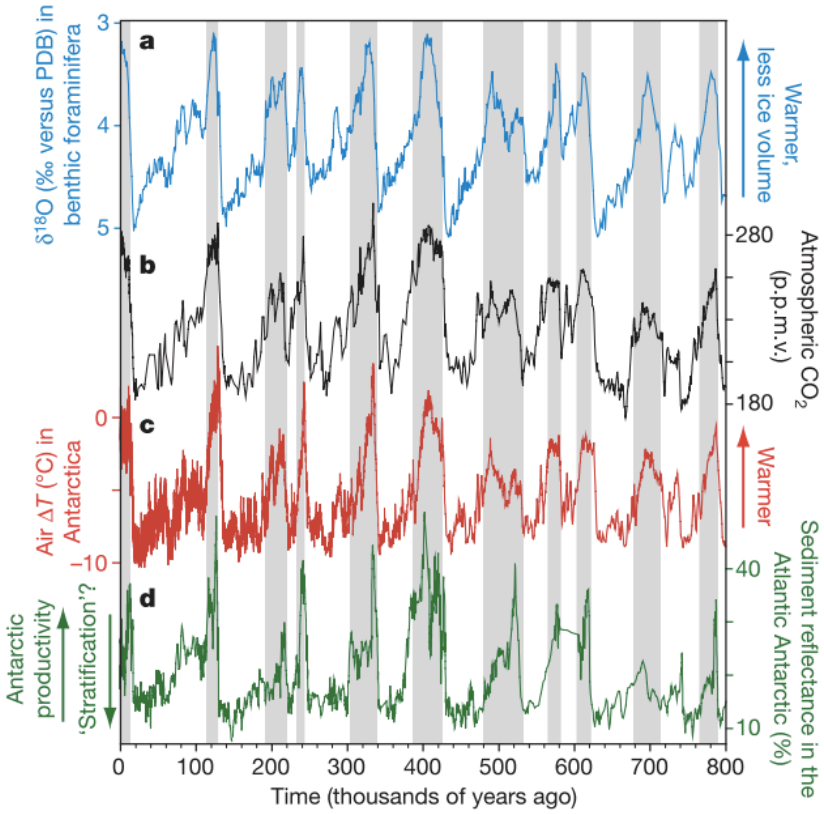

Fig. 1. Ice age cycles, including records of benthic $\delta^{18}O$, pCO_{2atm}, Antarctic temperatures and productivity. Low $\delta^{18}O$ (indicating warmer deep sea temperatures and small extent of continental ice sheets) are tightly coupled to high pCO_{2atm}, warmer Antarctica, and increasing Antarctic marine productivity, inferred from the higher reflectance of biogenic material (opal). Progressive cooling into glacial maxima and an abrupt deglacial rise in temperatures and pCO_{2atm} revealed the strong asymmetry of ice age cycles [*Sigman et al.*, 2010].

These observations fostered extensive efforts to understand the temporal evolution of the global carbon cycle and quantify fluxes between the various carbon reservoirs. On glacial-interglacial timescales three relatively reactive reservoirs are relevant. These are the

atmosphere with a carbon residence time of 7 years, the terrestrial biosphere (40 years) and the ocean, partitioned in surface (20 years) and deep ocean (1000 years) [*Hain et al.*, 2014]. The voluminous in earth's crustal reservoir has a residence time only relevant on geological timescales and is thus not further considered here. Carbon is exchanged between the atmosphere and land biosphere through photosynthesis/respiration and degradation of organic matter. Further, the air-sea gas exchange and the interaction between surface and deep ocean involves physical mixing, as well as biological processes. Another important component of the carbon cycle is the interaction between the ocean and $CaCO_3$ in marine sediments, explained further below. The carbon storage in the different reservoirs amounted to 600 PgC ($600*10^{15}$ grams of carbon) in the preindustrial atmosphere, 2100 PgC in the terrestrial biosphere, 700 PgC in the surface ocean and 38'000 PgC in the deep ocean [*Holmen*, 1992; *Hain et al.*, 2014]. With regard to the glacial-interglacial pCO_{2atm} change, it could be that either the terrestrial biosphere or the ocean (or both) compensated for the pCO_{2atm} variations. However, it has become clear that a glacial decrease rather than increase in terrestrial carbon storage was more likely and therefore cannot be linked to the decline in pCO_{2atm} [*Sigman and Boyle*, 2000]. Likewise, the reservoir sizes indicate that the ocean holds about 60 times more carbon than the atmosphere, and almost 20 times more than the terrestrial biosphere, wherefore only small changes in deep ocean carbon storage would greatly affect pCO_{2atm}. Thus it becomes clear that changes in pCO_{2atm} were driven to a large portion by changes in the ocean carbon storage, in particular by the large deep ocean reservoir [*Kohfeld and Ridgwell*, 2009; *Adkins*, 2013]. This involves several mechanisms including the biological pump and ocean circulation, which are explained in the next chapter.

2.2. Global and Southern Ocean circulation

This chapter should by no means address the global ocean circulation in its complicated and diverse nature, but rather provide an overview of the general structures required to understand glacial-interglacial changes. *Broecker* [1991] provided the simplified but useful picture of the ocean circulation represented as a large conveyor belt. The basic idea of the conveyor still holds true today, however, a more complicated and comprehensive picture has emerged. In general, water mass movements are driven by density gradients and atmospheric circulation. Variable heat and salt content in the water determines its buoyancy and fuels the so-called thermohaline circulation (THC) [*Rahmstorf*, 2002]. In addition, the THC is modified by large-scale atmospheric wind patterns, which transport surface water (Ekman Transport) thereby generating regions characterized by upwelling and downwelling systems, as well as surface currents within the upper ocean gyre systems[2] [*Lumpkin and Speer*, 2007; *Marshall and Speer*, 2012]. Fig. 2 illustrates a simplified circulation scheme from a SO perspective, covering the most distinct water masses and their flow routes.

[2] Gyres are large-scale ocean surface currents, induced by the prevailing wind patterns, coriolis force and boundary friction. Most prominent examples are the subtropical gyres, rotating clockwise in the NH and anti-clockwise in the SH, with an intensified western boundary current. [*Sarmiento and Gruber*, 2006].

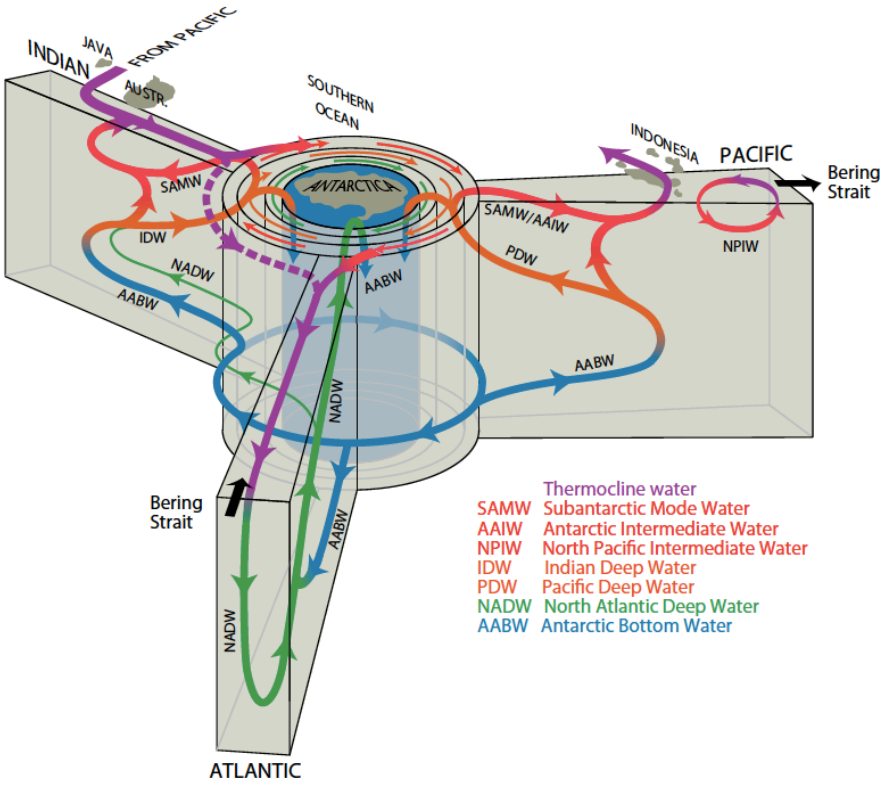

Fig. 2. Global ocean circulation centered around Antarctica. The SO basin connects waters formed in the three other major basins (Atlantic, Pacific and Indian Ocean). Deep waters sinking from the surface, only form in the North Atlantic (green arrows) and the SO (blue arrows). IDW and PDW (orange arrows) is deep water sourced from the ocean interior. Red and purple arrows indicate upper ocean and thermocline waters, respectively [*Talley*, 2013].

The following summary of the global ocean circulation is based to large parts on *Talley* [2013] with additions from other references. Relatively warm and salty water from the Atlantic subtropics is transported northwards by the western boundary current originating in the subtropical gyre system towards regions of deep water formation in the North Atlantic. Heat loss to the atmosphere reduces buoyancy, which allows the water mass to sink into depth, mainly within the Labrador Sea and the Nordic Seas where seasonal sea-ice further promotes downwelling. These "newly formed" waters flow southward as North Atlantic Deep Water (NADW). The resulting meridional overturning circulation causes a net heat transport to the North Atlantic by advection of warm surface water and southward outflow of colder deep water [*Lynch-Stieglitz et al.*, 2007]. On the way to the southern Atlantic, NADW mixes with Antarctic Bottom Water (AABW), the densest water mass in the ocean formed around the Antarctic continent, with main regions of deep water formation in the Ross and Weddell Sea. The mix of NADW and AABW is brought to the surface by wind-driven upwelling and surface buoyancy fluxes south of the Antarctic Circumpolar Current (ACC) system [*Marshall and Speer*, 2012]. The ACC is the largest ocean current driven by the strong SH westerlies and a lack of continental barriers [*Kuhlbrodt et al.*, 2007]. Around Antarctica, surface water is cooled to the freezing point and gets saltier due to brine rejection as a result of sea ice formation. These two processes allow AABW to sink to the bottom of the ocean. AABW then spreads northwards into the three ocean basins (Atlantic, Indian, Pacific). Besides AABW, the SO consists of circumpolar deep water (CDW) with an upper and lower component. CDW is a mixture of NADW, Pacific and Indian deep waters (PDW, IDW). Upwelled CDW is either

incorporated into northward flowing upper ocean water masses or joins the southward flow of NADW to form the dense AABW [*Talley*, 2013].

The Indo-Pacific Ocean has no analog of surface deep water formation because of enhanced surface stratification [*Talley*, 2013]. However, in the North Pacific there is a small overturning cell forming intermediate water masses. Deep water in the Indian and Pacific Ocean (IDW and PDW) results from interior ocean upwelling of southern sourced waters, including a fraction of NADW. IDW and PDW either mix with overlying upper ocean waters or flow southward, where they outcrop as CDW to the north of NADW upwelling regions. Subsequent northward Ekman transport represents the main source of the upper ocean water masses, Subantarctic mode water (SAMW) closer to the surface and further north respectively, and Antarctic intermediate water (AAIW). The northward flow of SAMW and AAIW into the Atlantic basin, along with upper ocean waters from the Agulhas leakage, Indonesian through-flow and Drake Passage, finally closes the global ocean conveyor [*Kuhlbrodt et al.*, 2007; *Talley*, 2013].

The circulation scheme described above results in distinct characteristics of water masses, altering their chemical properties and their ventilation history [*Sigman et al.*, 2010], which helps to discern between different water masses. The oldest (poorly-ventilated) water can be found in the northernmost reaches of the deep North Pacific with ages up to 2000 years, because NPDW was only partially ventilated in the SO, where NPDW had its last contact with the atmosphere. On the other hand, NADW and the surface ocean in general have a young ventilation age. The ventilation age can be inferred from radiocarbon measurements in water, with older water masses depleted in radioactive ^{14}C. [*Sarmiento and Gruber*, 2006]. An alternative way to identify water masses is through their chemical composition. In the Atlantic basin saltier NADW can be distinguished from the fresher, yet colder AABW, and in between the freshwater-tongue of AAIW is found, as AAIW originates from a region characterized by relatively fresh surface waters [*Talley*, 2013]. These chemical properties of water masses help to identify past changes in ocean circulation.

Due to the conjunction of most water masses in the SO and the complex interplay of currents, winds, buoyancy fluxes and water mass formation in characteristic zones and frontal systems, a closer look to this particular basin is necessary. In Fig. 3, a cross section through the SO with the Antarctic continent on the left side is illustrated. Relatively rapid upwelling of CDW, due to weak stratification arising from the small density difference throughout the water column, results in either a northward export of water masses as SAMW and AAIW respectively, or a southward flow and subsequent formation of dense AABW close to the continent [*Sarmiento and Gruber*, 2006]. On the top of Fig. 3, three zones are presented; (i) Antarctic Zone (AZ), (ii) the Polar frontal Zone (PFZ) and (iii) the Subantarctic Zone (SAZ), separated by the corresponding fronts, Antarctic Polar Front (APF), Subantarctic Front (SAF) and Subtropical Front (STF) furthest to the north. The STF represents the northern boundary of the SO basin and is defined by a large temperature gradient over a small latitude band (about 4°C over 0.5°), varying regionally and seasonally [*Orsi et al.*, 1995].

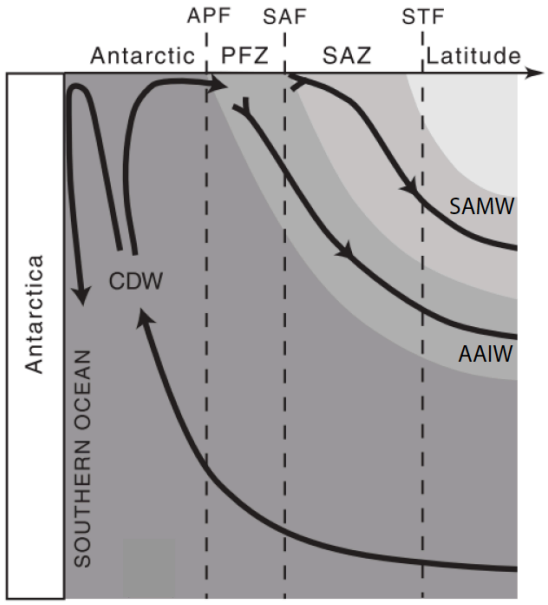

Fig. 3. Upwelling of deep waters and subsequent export in the SO. On top the distinct SO fronts, Antarctic Polar Front (APF), Subantarctic Front (SAF) and Subtropical Front (STF) are indicated, with the Antarctic continent on the left side. Upwelling of CDW south of the APF either forms AABW close to Antarctica or is incorporated into AAIW and SAMW further to the north (modified after Sarmiento et al., 2004).

In the SAZ, formation of SAMW occurs, which is then transported into the tropics. In the PFZ south of the SAF formation of AAIW with its characteristic low-salinity tongue takes place [*Sarmiento et al.*, 2004]. The APF is defined by a maximum temperature of 2°C above 200 meters, which represents the northernmost boundary of upwelling [*Orsi et al.*, 1995]. The upwelling in the northern AZ and sinking of AABW in the southern AZ close to the continent is of particular importance, as it is the window, where the deep ocean communicates with the atmosphere [*Adkins*, 2013]. Hence, also the exchange of carbon is largely controlled by the SO, which is more obvious, if the marine carbon cycle is considered [*Sigman et al.*, 2010].

2.3. Marine carbon cycle

As outlined above, it is widely accepted that the ocean modulated pCO_{2atm} variations on glacial-interglacial timescales. The marine carbon cycle offers several pathways to alter the carbon storage in the ocean interior, as it is characterized by a complex interaction between ocean physics, biology and chemistry. The majority of carbon in the ocean is present as inorganic compounds; bicarbonate ion (HCO_3^-), carbonate ion (CO_3^{2-}) and dissolved CO_2, referred collectively as dissolved inorganic carbon (DIC) [*Carlson et al.*, 2001]. The remainder is organic carbon (C_{org}) produced in the surface ocean by photosynthesis and $CaCO_3$ formed by calcifying marine organisms. Carbon chemistry allows the ocean to hold much more carbon than the atmosphere. Therefore, variations in pCO_{2atm} due to a terrestrial biosphere carbon loss would be largely balanced by the ocean's buffer capacity (see below). According to Eq. 1, gaseous CO_2 dissolves in water (H_2O) and reacts to produce carbonic acid (H_2CO_3), which rapidly dissociates into bicarbonate and carbonate ions [*Sarmiento and Gruber*, 2006].

$$CO_2 + H_2O \rightleftharpoons H_2CO_3^* \rightleftharpoons HCO_3^- + H^+ \rightleftharpoons CO_3^{2-} + 2H^+ \quad \text{(Eq.1)}$$

Note that $H_2CO_3^*$ refers to both carbonic acid and dissolved CO_2. The consequence of dissociation is that almost 90% of carbon in the ocean is present as HCO_3^-, about 10% as CO_3^{2-} and only 0.5% as $H_2CO_3^*$. Alkalinity (ALK) defined as the excess of bases over acids in the water, determines the ocean's buffer capacity, which allows $H_2CO_3^*$ to dissociate into the other DIC components. To a first approximation, ALK can be seen as the sum of HCO_3^- and twice CO_3^{2-}, as the carbonate ion is twice as negatively charged and can accept two protons. The relative abundance of the DIC components depends on water pH. A lower pH (higher acidity) forces reactions in Eq. 1 to the left hand side, increasing $H_2CO_3^*$ and therefore oceanic CO_2 concentrations (pCO_{2oc}). From the definitions of ALK and DIC, it can be inferred that the concentration of CO_3^{2-} is roughly determined by the difference of ALK and DIC [*Sarmiento and Gruber*, 2006].

The exchange of carbon between the ocean and the atmosphere naturally only takes place at the surface ocean-atmosphere interface. The direction of the carbon flux is determined by the pCO_2 difference of the two reservoirs. If pCO_{2oc} is lower/higher than pCO_{2atm}, then CO_2 enters/leaves the ocean, having an equilibration time of several months [*Sarmiento and Gruber*, 2006]. Parameters that influence pCO_{2oc} thus need to be addressed in detail. These parameters are the concentration of ALK, DIC, the salinity content and temperature. From the above it becomes clear that a higher ALK lowers pCO_{2oc} due to increased dissociation of $H_2CO_3^*$. In contrast a higher DIC content in the water raises pCO_{2oc}. According to Henry's Law the solubility of a gas decreases with increasing temperature. An increase in ocean temperature of 1°C, raises pCO_{2oc} by about 4% [*Carlson et al.*, 2001]. Likewise a higher salinity increases pCO_{2oc}, but due to the large temperature variations in the global ocean, salinity is of lesser importance [*Sarmiento and Gruber*, 2006]. Temperature is only a physical property while DIC and ALK are influenced by biology simultaneously, thus a separation between these two is helpful. Temperature-induced pCO_{2oc} variations are referred to the solubility pump, whereas the redistribution of DIC and ALK is determined by the biological pump, further divided into the soft tissue pump and the carbonate pump [*Kohfeld and Ridgwell*, 2009].

The solubility pump is driven by ocean surface temperature variations, because cold water has a higher solubility for CO_2 [*Kohfeld and Ridgwell*, 2009]. Thus, solely considering the global ocean temperature distribution, colder oceans in mid- to high latitudes take up CO_2, whereas in the warmer (sub)-tropics CO_2 is outgassed from the ocean. The pump results from ocean circulation with deep water formation in cold regions, pumping CO_2-rich water into depth. Consequently the ocean interior is filled with cold relatively CO_2-rich water, which lowers pCO_{2atm} [*Hain et al.*, 2014].

2.3.1. Soft tissue vs. carbonate pump

The ocean does not have a large biomass reservoir like the terrestrial biosphere, wherefore only little organic matter accumulation occurs. However, the production of C_{org} and $CaCO_3$ by marine organisms redistributes DIC and ALK between the surface and interior ocean, defining the story line of the biological pump [*Hain et al.*, 2014]. As they affect pCO_{2oc} (and

in turn pCO_{2atm} through equilibration) in opposing ways, it is important to clearly distinguish between the soft tissue pump, which cycles C_{org}, and the carbonate pump, which drives the $CaCO_3$ cycle [*Kohfeld and Ridgwell*, 2009]. The general concept of the soft tissue pump is depicted in Fig. 4 with the cycling of C_{org} and nutrients between the surface and deep ocean [*Sarmiento and Gruber*, 2006]. Phytoplankton in the surface ocean converts inorganic carbon into C_{org} by means of photosynthetic activity, thus lowering DIC and producing O_2. Among others, phytoplankton mainly require macronutrients (phosphate, nitrate and silicate), iron (Fe) and light. As light decreases rapidly with depth, photosynthesis is only possible in the euphotic zone of the ocean, that is the upper 100-150 meters [*Carlson et al.*, 2001]. The larger fraction of C_{org} never exits the surface ocean owing to rapid remineralization and is consequently insignificant to the soft tissue pump. About 10 – 50 % of C_{org} sinks out of the sunlit surface ocean, where it is ultimately decomposed by bacteria and grazing organisms. In sediments only about 1% of initially produced C_{org} accumulates, a process that becomes relevant on geological timescales [*Hain et al.*, 2014]. Remineralization breaks C_{org} down into nutrients and DIC, simultaneously consuming dissolved O_2 thereby increasing the DIC and nutrient content of the deep ocean. By virtue of upwelling, nutrients and DIC are brought back to the surface ocean, where the cycle starts again [*Sarmiento and Gruber*, 2006].

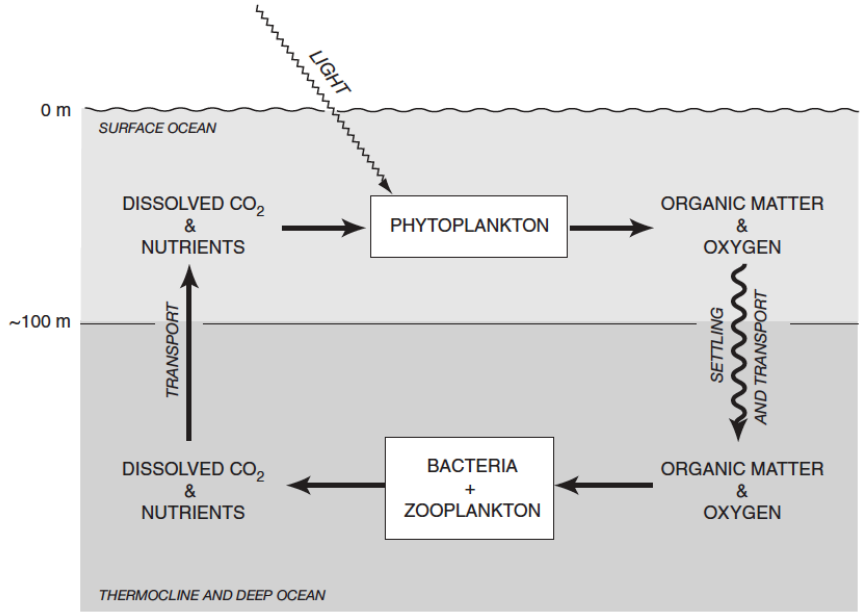

Fig. 4. Schematically illustrated biological pump (soft tissue component). In the euphotic zone (light gray layer), photosynthetic activity converts nutrient and DIC (written as dissolved CO_2) into organic matter (C_{org}) and releases O_2. Subsequent export of C_{org} into the ocean interior (dark gray layer) leads to remineralization by bacteria and grazing organisms, thereby O_2 is consumed. Ocean circulation finally brings nutrients and DIC back to the surface ocean. The temporal sequestration of DIC as C_{org} lowers pCO_{2oc} of the surface ocean, wherefore outgassing to the atmosphere is reduced [*Sarmiento and Gruber*, 2006].

An intuitive implication of this cycle would be that a higher biological activity helps to lower DIC in the surface causing a drawdown in pCO_{2oc}. However, it is the balance between upwelling nutrients/DIC and downward export of C_{org} that controls CO_2 exchange, which is often referred to as the efficiency of the soft tissue pump [*Sigman and Boyle*, 2000]. Separating the nutrient concentration into preformed (unused nutrients by biology and transported downwards by ocean circulation) and regenerated nutrients (originating from

remineralization of C_{org} within the interior ocean) provides a measure of this efficiency [*Hain et al.*, 2014]. The metric assumes that the ratio[3], by which phytoplankton in the surface ocean incorporates nutrients and carbon remains relatively invariant. Hence, for a certain stock of nutrients consumed, a corresponding, determined amount of carbon is incorporated into C_{org}. Consequently, high preformed nutrient contents at the time when water leaves the surface ocean inevitably speaks for a missed chance of carbon uptake and thus a low efficiency of the pump, resulting in a greater carbon leak (CO_2 outgassing) [*Sigman and Boyle*, 2000]. Alternatively formulated, the higher the fraction of upwelled nutrients consumed by phytoplankton, the more efficient the soft tissue pump works and pCO_{2atm} declines [*Hain et al.*, 2014].

As stated above the cycling of $CaCO_3$ needs to be considered individually. The formation of $CaCO_3$ in surface water decreases DIC and ALK in a 1:2 ratio, according to Eq. 2 [*Zeebe*, 2012].

$$Ca^{2+} + 2HCO_3^- \rightarrow CaCO_3 + CO_2 + H_2O \qquad \text{(Eq. 2)}$$

As ALK decreases more than DIC (Eq. 2) it becomes clear, that $CaCO_3$ formation and subsequent export into depth raises pCO_{2oc} of the surface ocean and consequently pCO_{2atm}. As a consequence the carbonate pump is often described as carbonate counter pump [*Zeebe*, 2012]. While a strong carbonate pump increases pCO_{2atm}, a strong soft tissue pump lowers pCO_{2atm}. However, in general it is believed that the implications of the soft tissue pump on pCO_{2atm} are more pronounced [*Hain et al.*, 2014]. In the deep ocean, $CaCO_3$ dissolution causes an increase in ALK and DIC again in a 2:1 ratio (Reverse of Eq. 2). The vertical partitioning of DIC and ALK by both pumps causes another process, relevant on glacial-interglacial timescales, that is the carbonate compensation (Alkalinity feedback). Riverine input of ions and the fraction of $CaCO_3$ buried in ocean sediments (about 25% of initial production) maintain the ALK balance in the ocean [*Hain et al.*, 2014]. The depth of the lysocline, below which almost all $CaCO_3$ is dissolved, determines the global burial rate of $CaCO_3$. The lysocline in turn is controlled by the concentration of CO_3^{2-}. If the concentration is below $CaCO_3$ saturation concentration, which increases with depth (pressure), then $CaCO_3$ gets dissolved. Transient deepening or shoaling of the lysocline is called carbonate compensation, since the initial, transient imbalance in the ALK budget is compensated by $CaCO_3$ burial on the seafloor [*Sigman et al.*, 2010]. Changes in the soft tissue pump and the carbonate pump affect this equilibrium, via the redistribution of ALK and DIC and in turn the depth of the lysocline [*Sigman and Boyle*, 2000]. A stronger soft tissue pump directly lowers pCO_{2oc} in the surface by transferring DIC into the interior ocean. Additionally, the higher DIC content decreases the deep ocean pH value and thus decreases the CO_3^{2-} concentration there (see Eq. 2), which shoals the lysocline. Shoaling of the lysocline decreases the sea floor area, where $CaCO_3$ is preserved and buried. As a consequence less $CaCO_3$ burial occurs, thereby increasing whole ocean ALK, because the riverine input is assumed to have remained constant. While the increase in whole ocean ALK causes an increase in deep CO_3^{2-} concentration until initial $CaCO_3$ burial is resettled, it simultaneously lowers pCO_{2atm}, enhancing the effect of a stronger soft tissue pump [*Sigman et al.*, 2010].

[3] Redfield Ratio: C:N:P:O_2 = 106:16:1:-138, meaning for 1 mol consumed phosphorus (P), 16 mol of nitrogen (N) and 106 mol of carbon (C) are consumed and 138 mol oxygen (O_2) are released [*Sarmiento and Gruber*, 2006].

2.4. Marine carbon cycle linked with ocean circulation

The size of the deep ocean nutrient- and DIC reservoir is determined by a combination of organic matter remineralization kinetics and ocean circulation (Fig. 5). As soon as water leaves the surface layer, nutrients and DIC start accumulating. As a result aged water masses in the deep Pacific and Indian Ocean hold high nutrient and DIC concentrations due to their long exposure to organic material remineralization [*Sigman et al.*, 2010]. The nutrient content of water masses brought to the surface is crucial for surface productivity. Therefore it is important to connect the marine carbon cycle with key regions of global ocean circulation. The deep ocean, carrying the lion's share of ocean carbon storage, is filled with water formed in the North Atlantic (NADW) and the AZ (AABW). Thus the relative contribution of these two end members in ventilating the deep ocean mainly control the preformed nutrient concentration of the interior ocean [*Hain et al.*, 2014]. Northern sourced deep waters carry very little preformed nutrients, as it is stemming from surface waters, which has circulated throughout the surface Atlantic, where its exposure to biological activity has depleted its nutrient stock. On its pathway to the south, NADW progressively accumulates regenerated nutrients and DIC from remineralization of sinking C_{org} [*Sigman et al.*, 2010].

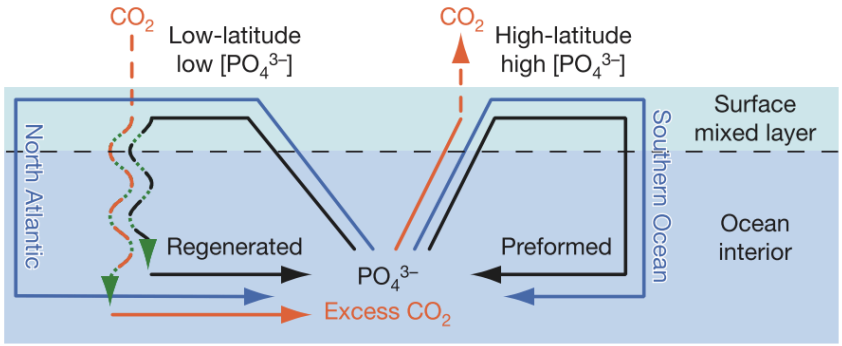

Fig. 5. Contrasting the efficiency of the soft tissue pump in the North Atlantic and the SO. Blue arrows illustrate ocean circulation with the transport of macronutrients (nitrate and phosphate) indicated by the black arrows. On its pathway to the North Atlantic, nutrients in surface waters (light blue layer) are almost completely consumed owing to the high biological productivity in low latitudes, leaving no room for preformed nutrients to sink into the ocean interior (dark blue layer). This lowers surface pCO_{2oc} wherefore CO_2 from the atmosphere invades (stippled orange arrow). In contrast in the SO, incomplete nutrient consumption fills the ocean interior with preformed nutrients, causing high surface pCO_{2oc} and CO_2 outgassing into the atmosphere. The excess CO_2 in the ocean interior origins from remineralization of sinking C_{org} (wavy arrows), also creating a pool of regenerated nutrients. Thus the ratio of regenerated to preformed nutrients is a measure for the efficiency of the soft tissue pump [*Sigman et al.*, 2010].

In contrast, the SO marks the region where water with the highest preformed nutrient concentration is transferred to greater depths, resulting from incomplete nutrient consumption by phytoplankton due to the scarcity of micronutrient Fe and light availability. Around the ACC nutrient and carbon-rich deep water is rapidly brought to the surface and exported to depth in the AZ, or transported northwards as SAMW and AAIW north of the APF (see section ocean circulation). The AZ and the SAZ are both characterized by a high abundance of dissolved nitrate, phosphate and partially silicate [*Sarmiento et al.*, 2004]. Despite the high surface nutrient concentration, relatively low photosynthetic activity is observed in this region, thus the SO acquired the name of a high nutrient, low chlorophyll region (HNLC)

[*Kohfeld and Ridgwell*, 2009]. The northward export of water masses having origin in the SO is of less importance, as these do not ventilate much of the interior ocean, although they can generate important feedback mechanisms in low latitude ecosystems [*Matsumoto et al.*, 2002; *Sarmiento et al.*, 2004]. On the other hand, formation of AABW with a high preformed nutrient concentration ventilates a large part of the deep ocean. The unused nutrients indicate that not all DIC is converted to C_{org}, leaving surface pCO_{2oc} at higher levels (Fig. 5). [*Sigman and Boyle*, 2000]. In summary, the SO, in particular the AZ, is seen as the key driver of glacial-interglacial changes in pCO_{2atm}, because of the leverage imposed on the global efficiency of the biological pump, which controls the partitioning of CO_2 between the ocean and the atmosphere [*Sigman et al.*, 2010; *Hain et al.*, 2014]. The idea of the SO's dominant role in controlling pCO_{2atm} is certainly not new. Early climate modeling studies from the so-called Harvardton Bears box models [*Knox and McElroy*, 1984; *Sarmiento and Toggweiler*, 1984; *Siegenthaler and Wenk*, 1984] revealed that polar biological productivity and deep ocean ventilation were key drivers of carbon exchange between deep ocean and atmosphere [*Adkins*, 2013].

2.5. Glacial-interglacial changes – general processes

Before carefully examining the changes in ocean biology and circulation with an emphasis on the SO, an overview of other parameters that influence pCO_{2atm} are provided. The following mechanisms and estimates of pCO_{2atm} change are summarized based on *Sigman and Boyle* [2000] and *Kohfeld et al.* [2005] (for more details see corresponding articles and references therein). The role of the terrestrial biosphere is not specifically addressed, despite having contributed to an estimated increase in pCO_{2atm} of about 22 ppmv during ice ages. Terrestrial carbon storage decrease is thought to be a combination of less vegetation cover due to extensive ice sheets and a generally drier climate during cold periods. The initial pCO_{2atm} would have been larger, but owing to the ocean's buffer capacity and carbonate compensation the impact of terrestrial carbon loss was diminished [*Kohfeld and Ridgwell*, 2009].

The most straightforward influence on pCO_{2atm} relates to the generally colder oceanic temperatures during ice ages. Since the solubility of CO_2 increases with decreasing water temperatures, global cooling caused pCO_{2atm} simultaneously to decline. Estimates of the glacial cooling show high regional variability with an average of about 2 – 4 °C [*Sarmiento and Gruber*, 2006]. At high latitudes, where the deep ocean is ventilated, glacial ocean temperatures were about 2.5°C lower, causing a pCO_{2atm} drawdown of roughly 30 ppmv [*Sigman and Boyle*, 2000]. The second, relatively simply ascertainable glacial pCO_{2atm} driver was the lower sea level form freshwater storage on continental ice sheet. Enhanced ice volume increased salinity by about 3%, as well as DIC and ALK in a 1:1 ratio. While higher salinity and DIC, increases pCO_{2oc} and thus CO_2 outgassing to the atmosphere, higher ALK lowers pCO_{2oc}. The contribution of these 3 effects results in a pCO_{2atm} increase of about 13 ppmv [*Kohfeld and Ridgwell*, 2009]. Despite uncertainties in all these estimates, it becomes inevitably clear that other processes must have caused lower glacial pCO_{2atm}, as the addition of the individual processes outlined above results in a near zero change of pCO_{2atm} [*Sigman and Boyle*, 2000].

Decades of paleoceanographic research have provided numerous hypotheses, trying to resolve pCO_{2atm} drawdown, which involve an altered ocean circulation and/or a change in biological processes [*Rahmstorf*, 2002]. To discuss all of these in detail would go beyond the scope of this thesis. The focus lies clearly on changes in the SO, due to its key role on the biological pump. However the SO is not isolated from the global ocean and thus processes are interwoven with changes in other regions [*Sigman et al.*, 2010]. In the following, possible mechanisms that contribute to weaken CO_2 outgassing in the SO and thus increase ocean's carbon storage during glacial periods are discussed. The processes can be separated into two groups, one involving changes in marine biology and the other physical changes in ocean circulation [*Sigman and Boyle*, 2000].

2.5.1. Glacial changes in Southern Ocean's biological productivity

The reasoning outlined above highlights the strong sensitivity of pCO_{2atm} to changes in the SO. However, it is worth mentioning that export production also faced significant glacial-interglacial changes in other parts of the ocean. For example, biological productivity in the tropical Atlantic was likely larger during glacial maximums [*Kohfeld et al.*, 2005]. Yet, as nutrient consumption in these regions is nearly complete today, higher export production must have resulted from a higher nutrient supply and thus has no net effect on pCO_{2atm} [*Sigman and Boyle*, 2000]. On the other hand, a change in the composition of the exported matter, namely a different C_{org}:$CaCO_3$ rain ratio would affect pCO_{2oc} and in turn pCO_{2atm}, due to the individual impacts of the respective pumps on ALK and DIC concentrations. This aspect will be further discussed below. In the following, it is referred to the soft tissue component, as the region south of the SAF is dominated by C_{org} export of non-calcifying organisms [*Hain et al.*, 2014]. However it needs to be realized that corresponding changes in $CaCO_3$ export could lessen the impact of the soft tissue pump on pCO_{2atm} [*Hain et al.*, 2010; *Salter et al.*, 2014].

In order to explain lower pCO_{2atm}, early hypothesis proposed an overall increase of SO's export production during glacial periods [*Sarmiento and Toggweiler*, 1984]. However, regional differences of lower [*Mortlock et al.*, 1991] and higher [*Kumar et al.*, 1995] productivity in different regions of the SO were identified. An integration of the Atlantic sector of the SO revealed no significant changes in export production [*Frank et al.*, 2000]. This study generally showed an increase in export production north of the APF compensated by a decline south of the APF during ice ages. From growing evidence of observations, a highly consistent picture of higher glacial C_{org} export in the SAZ and lower export in the AZ has emerged [*Kohfeld et al.*, 2005; *Jaccard et al.*, 2013]. Reconstructions of export production are based on different proxies, such as opal, biogenic barium or carbonate fluxes, an approach that will be discussed in detail in the Proxies chapter.

Today the region south of the APF coincides with the so-called opal belt, where a large portion of the global opal burial from silicifying diatoms occurs [*Frank et al.*, 2000]. These authors observed that during glacials, the opal belt faced significant northward movement, consistent with a reduction in export production south of the APF. Additionally, analysis of Nitrogen isotopes ($\delta^{15}N$), a proxy for the degree of nitrate consumption, revealed a higher glacial nutrient utilization in the AZ [*Francois et al.*, 1997; *Studer et al.*, 2015]. Phytoplankton preferentially assimilate nutrients with lighter isotopes, in this case nitrate with

^{14}N. With enhanced nutrient depletion, surface nitrate gets relatively enriched in ^{15}N, whereby the higher $\delta^{15}N$-signal is incorporated into organic matter [*Altabet and Francois*, 1994]. A decreased export production in concert with enhanced nutrient consumption was only possible with a decline in subsurface nutrient supply to the AZ, resulting from a modified ocean circulation/stratification [*Francois et al.*, 1997].

The SAZ underwent a different evolution. There, increased glacial export production has been observed during glacial times [*Kohfeld et al.*, 2005]. The direction of change in nutrient utilization has been more difficult to assess. While earlier analysis found a slight decrease in nutrient utilization north of the APF during glacials, meaning lower $\delta^{15}N$ values [*Francois et al.*, 1997], this finding has been revised recently. Isotope measurements on individual diatoms and foraminifera species, which is thought to be more accurate than measurements on bulk sediment, has revealed a pronounced glacial $\delta^{15}N$ increase and thus a higher degree of nutrient consumption in the SAZ [*Robinson et al.*, 2005; *Robinson and Sigman*, 2008; *Martínez-García et al.*, 2014]. As noted above, modern biological productivity is limited by Fe supply in large parts of the global ocean [*Hain et al.*, 2014]. It was John Martin [*Martin*, 1990] who proposed the "Iron-Hypothesis" as a possible explanation to the glacial CO_2 problem. Under a generally drier climate, eolian Fe-bearing dust supply to the ocean (and Antarctica, where ice cores recorded the dust signal) was enhanced [e.g., *Lambert et al.*, 2008]. This may lead to a higher biological activity in the ocean and consequently an increase in the degree of nutrient consumption. Fe fertilization is of particular importance within the SAZ and the SO in general, as this region lies downwind of the major dust sources; Australia, South America and South Africa [*Lamy et al.*, 2014]. However, the increase in glacial export production could result either from a higher nutrient consumption or an increased subsurface nutrient supply or both [*Sigman and Boyle*, 2000].

2.5.2. Southern Ocean circulation during glacial times

The proposed changes in glacial nutrient supply to the surface were linked to a modified upwelling system in the SO. Modern upwelling in the AZ is controlled by SH westerly winds, which result in a northward Ekman transport of water masses, counteracting eddy fluxes that largely balance the wind-driven upwelling and buoyancy forcing, resulting from air-sea heat fluxes as well as sea ice induced freshwater fluxes [*Marshall and Speer*, 2012]. From the paleoceanographic data discussed above, it has been inferred that subsurface nutrient supply and consequently upwelling in the AZ was substantially reduced during glacial times [*Sigman and Boyle*, 2000]. There are contrasting views about the ultimate causes responsible for decreased glacial upwelling in the AZ [*Watson and Naveira Garabato*, 2006]. One hypothesis invokes a northward displacement of the westerly wind belt during colder periods, related to a reorganization of the large-scale atmospheric circulation [*Toggweiler et al.*, 2006; *Anderson et al.*, 2009]. The subsequent reduction of Ekman transport in the AZ would directly decrease upwelling. Indirectly, less upwelling of salty NADW lowered the dissipation of the relatively fresh surface water (halocline), promoting Antarctic surface stratification. Another theory suggests that colder climate was accompanied by a sea ice induced salinity stratification of the AZ [*Sigman and Boyle*, 2000]. The enhanced surface stratification in the AZ would provoke less overturning in the SO [*Sigman et al.*, 2010].

It needs to be mentioned that no clear picture of the change in the westerly winds has emerged yet [*Kohfeld et al.*, 2013], and it has been argued that modified buoyancy fluxes were responsible for the decreased glacial upwelling, rather than AZ stratification or modified westerlies, whose effects would be buffered by countering eddies [*Watson and Naveira Garabato*, 2006]. These authors proposed that colder temperatures coupled with increased sea ice coverage reduced the air-sea heat flux, whereby buoyancy was lost and upwelling declined. In the modern ocean, besides upwelling of deep waters also vertical mixing supplies nutrients to the AZ. [*Lourey and Trull*, 2001]. More pronounced AZ stratification during glacial periods would have reduced subsurface nutrient supply owing to weaker vertical mixing, enhancing the effect of decreased upwelling [*Jaccard et al.*, 2013]. Supposed the northward shift of the westerly winds occurred, stronger upwelling and higher nutrient supply to the SAZ would be a direct consequence. This could explain a part of the higher export production there, possibly modified by Fe Fertilization [*Sigman and Boyle*, 2000; *Martínez-García et al.*, 2014].

2.5.3. Global ocean circulation during glacial times

Reconstructing the glacial ocean circulation by itself is a tremendous area of research. Consecutively only the most prominent features of the glacial circulation, relevant for the biological pump's efficiency, are summarized. NADW formation was not much weaker during most of the last glacial period [*Lippold et al.*, 2012], however, a shoaling of its depth penetration has been observed at the LGM, leading to the name of glacial North Atlantic intermediate water (GNAIW) [*Lynch-Stieglitz et al.*, 2007]. On the other hand, the circulation proxy $^{231}Pa/^{230}Th$ documented an almost complete shutdown in northern sourced deep waters during Heinrich-events, which were extreme NH stadials, likely triggered by a large freshwater flux to the North Atlantic due to a partially collapsing ice sheet [*Böhm et al.*, 2015]. As a consequence, a larger fraction of the deep ocean was filled by AABW during the LGM, which also entered the deep North Atlantic [*Lynch-Stieglitz et al.*, 2007]. In contrast, it seems that deep water ventilation in the AZ and thus AABW formation was reduced during most of the glacial period, wherefore several hypotheses have been invoked [*Sigman et al.*, 2010]. Possible causes are the wind- or sea ice induced surface stratification in the AZ [*Sigman and Boyle*, 2000], a stronger stratified deep ocean (see below) with less interior mixing and different surface buoyancy fluxes [*Watson and Naveira Garabato*, 2006; *Adkins*, 2013], or the increasing importance of surface salinity stratification in polar regions under colder climatic conditions [*Sigman et al.*, 2004]. In summary a decreased overturning in the SO seems reasonable, even though the exact mechanism yet remains unclear.

A more coherent picture is provided for the glacial deep ocean, which has appeared to be more vertically stratified compared to modern times. Global cooling caused the deep ocean vertical structure to be controlled predominantly by salinity and less by temperature during glacial periods, resulting from the increased density dependence on salinity at low temperatures [*Sigman et al.*, 2004; *Adkins*, 2013]. Presently, AABW and NADW mixing in the deep ocean is vigorous. Compared to AABW, the relatively warm and salty NADW is denser at the surface, yet less dense in deeper waters due to its heat content, which leads to a

sharing of isopycnals[4] between both water masses, whereby mixing is promoted. However, in glacial periods the salinity gradient between AABW and NADW was reversed. Due to intensified brine rejection and possibly less sea ice melting as colder water upwelled around Antarctica, AABW became more saline during glacial periods [*Adkins*, 2013]. In turn deep ocean mixing was reduced, as it required more energy to mix across isopycnals [*Watson and Naveira Garabato*, 2006]. Topographic features, e.g. mid ocean ridges are an additional driver of deep mixing. With a shoaling of the contact between AABW and GNAIW, less topographical induced mixing of the deep ocean occurred during peak ice ages [*Adkins*, 2013]. The decline in deep ocean mixing could have promoted the accumulation of the uniquely dense glacial AABW in the deep ocean, reducing its need to form and thus decreased Antarctic overturning during glacial periods [*Sigman et al.*, 2010].

2.6. Implications of glacial productivity/circulation changes on pCO_{2atm}

As stated above, the rapid subsurface nutrient supply in the AZ combined with incomplete nutrient consumption accounts for the biggest leak in the modern biological pump [*Martínez-Garcia et al.*, 2011]. Even though total export production during glacial periods was lower, declining nutrient supply lead to a more complete consumption in the AZ, reducing CO_2 outgassing [*Sigman and Boyle*, 2000]. More complete consumption could be the result of AZ surface stratification and a shallower mixed layer, enhancing light availability for phytoplankton, which today also represents a major limiting factor of productivity [*Robinson et al.*, 2005]. Alternatively enhanced Fe supply to the AZ may also be a reasonable explanation. Although the dominant Fe supply route to the AZ is from subsurface waters and not via eolian transport, either an increasing Fe-to-nutrient ratio in upwelled water (resulting from globally enhanced dust input) or directly enhanced eolian Fe fluxes could have increased nutrient consumption and closed the AZ leak at least partially [*Martínez-Garcia et al.*, 2011]. Yet questions about the availability of dust-bearing Fe have been raised [*Parekh et al.*, 2008; *Fischer et al.*, 2010]. Irrespective of the exact mechanism, higher nutrient utilization in the AZ lowered the preformed nutrient concentration transferred to depth, which indicates a higher efficiency of the biological pump [*Sigman et al.*, 2010]. Changes in the AZ are capable of explaining a fraction of the decreased glacial pCO_{2atm} concentration with estimations up to 40 ppmv [*Hain et al.*, 2010; *Jaccard et al.*, 2013].

The increased export production and nutrient utilization in the SAZ was most likely due to a combination of higher nutrient supply and Fe fertilization [*Martínez-García et al.*, 2014]. Nevertheless, this has not largely affected the efficiency of the biological pump, because AAIW and SAMW ventilate a smaller fraction of the global ocean [*Sigman et al.*, 2010]. Thus a decline in AAIW/SAMW preformed nutrient concentrations would only result in modest changes in oceanic CO_2 storage. SAZ productivity changes, however, could have induced feedback mechanisms including carbonate compensation. Higher C_{org} export to the ocean interior and subsequent remineralization, may have increased the deep ocean DIC content and as a result shoaled the lysocline depth [*Sigman and Boyle*, 2000]. The transient total increase in ocean ALK would help to sequester more CO_2 in the ocean interior. Another way to influence CO_2 storage in the ocean is by changing the rain ratio of C_{org}:$CaCO_3$,

[4] lines of equal density

meaning a change in the strength of the carbonate pump relative to the soft tissue pump [*Kohfeld and Ridgwell*, 2009]. Today most of the $CaCO_3$ export takes place in the (sub)tropical regions, whereby CO_2 outgassing is favored by reduced surface ALK [*Hain et al.*, 2014]. A hypothesis to reduce the strong tropical carbonate pump is provided by the silicic acid leakage hypothesis (SALH), which states that in glacial periods diatom productivity at low latitudes was enhanced at the expense of calcifying organisms [*Matsumoto et al.*, 2002]. Excess silicate might be transported to the tropics due to decreased opal production in the AZ as well as a decreased silicate to nitrate (Si:N) uptake ratio in the SO as a result of Fe fertilization [*Brzezinski et al.*, 2002]. Including these feedbacks, the increase in SAZ export production could be capable of decreasing pCO_{2atm} by another 40 ppmv [*Hain et al.*, 2010; *Martínez-García et al.*, 2014]. This two modes of changes in the SO were reconstructed from sediment archives, where the timing of productivity changes in the AZ and SAZ match consistently the changes in pCO_{2atm} [*Jaccard et al.*, 2013].

Deep ocean changes represent the final jigsaw piece to constrain the glacial biological pump. We have learnt that the glacial deep ocean was more stratified, resulting in the accumulation of regenerated nutrients and DIC. Evidence for this is provided by benthic foraminiferal $\delta^{13}C$, which works similar to $\delta^{15}N$. Phytoplankton in the surface preferentially consume the lighter isotope ^{12}C leaving the surface ocean enriched in ^{13}C. In the interior ocean, remineralization of C_{org} increases ^{12}C relatively over ^{13}C leading to a $\delta^{13}C$ decline [*Kohfeld and Ridgwell*, 2009]. The deep glacial Atlantic was apparently filled with depleted $\delta^{13}C$ southern sourced water, which indicates a higher regenerated nutrient content [*Curry and Oppo*, 2005]. Besides that, a shift of the oxygen minimum from mid-depth into the deep ocean was inferred in various regions of the world ocean [*Jaccard et al.*, 2009; *Jaccard and Galbraith*, 2012]. This could either indicate increased C_{org} remineralization in depth owing to higher productivity, since this consumes oxygen, or declined deep ocean ventilation, as a result of Antarctic stratification and shallower GNAIW. Both mechanisms would cause a drawdown in pCO_{2atm}. Similarly, in the deep Atlantic higher regenerated nutrient concentrations and a lower oxygen content during the last glacial, in particular at the LGM, were found, which argues for a higher efficiency of the soft tissue pump [*Hoogakker et al.*, 2015]. The enhancement of nutrients and DIC in the deep ocean would again promote carbonate compensation, storing additional CO_2 in the ocean. In relation to deep ocean ventilation, a relative shift of northern sourced to southern sourced water masses at the LGM would increase interior ocean's preformed nutrient concentration. However, this change seems to be compensated by higher nutrient consumption in the SO, a decrease in preformed nutrients of GNAIW, and higher regenerated nutrient and DIC accumulation in the deep ocean [*Sigman et al.*, 2010]. Additionally, an increase in southern sourced water masses is not inevitably accompanied by a proportional increase in AZ ventilation [*Hain et al.*, 2010]. AABW filling the deep ocean might have been last ventilated in the North Atlantic, which is supported by increased glacial ventilation ages in the deep SO [*Skinner et al.*, 2010]. Ventilation in the AZ was probably impeded by surface stratification and/or enhanced sea ice coverage, thus glacial AABW seemingly had less contact with the surface Antarctic, which is consistent with decreasing export production from the AZ [*Hain et al.*, 2010].

2.7. Motivation and approach of the master thesis

From the above reasoning it is clear that a variety of hypotheses exist, trying to explain the origin and dynamics of ice age cycles. The particular importance of the SO in terms of controlling natural pCO_{2atm} variations on glacial-interglacial timescales has become evident in recent years [*Sigman et al.*, 2010; *Hain et al.*, 2014]. An important contribution to these finding has arisen from marine sediment cores, which provide the possibility to reconstruct past changes in ocean biogeochemistry. By analyzing the general composition and individual constituents, it is possible to infer variations over time within the overlying water mass. Biological export production (BEP) can be reconstructed by the combination of different proxy records, which is more reliable due to the individual preservation characteristics of sedimentary components. As the biological pump is thought to be the key driver of past variations in pCO_{2atm}, reconstructing BEP as well as nutrient supply is crucial to infer its leverage on pCO_{2atm} in the past [*Sigman and Boyle*, 2000].

Several studies with sediment cores from the SO revealed the high variability of BEP over glacial periods in the Atlantic sector [e.g., *Frank et al.*, 2000; *Anderson et al.*, 2009; *Jaccard et al.*, 2013; *Martínez-García et al.*, 2014] or in the central Pacific sector [*Lamy et al.*, 2014; *Studer et al.*, 2015]. Likewise, changes of BEP from the LGM to the Holocene are relatively well constrained for the global SO [*Kohfeld et al.*, 2005]. Yet, there is a lack of high-resolution data covering a full glacial cycle in some other SO regions. In this thesis, sediment core SO136-111 from the western Pacific sector of the SO was investigated, covering the last 150 kyr. The core was retrieved from the sensitive APF, where distinct changes in marine biology and ocean circulation over glacial-interglacial cycles are expected. The sedimentation rate should also allow detecting millennial scale events. Here, a multi-proxy-approach, meaning the combination of individual measures of biological activity nutrient supply and deep water oxygenation is provided. These analyses should help to reconstruct BEP and deep ocean ventilation in the SW Pacific, thus constraining the biological pump's efficiency in this region. Export fluxes of opal, $CaCO_3$, biogenic barium (bioBa) were generated by ^{230}Th-normalized sedimentation rates, which together provide a conclusive measure of productivity. As opal fluxes are mainly driven by the rate of silicate supply to the AZ surface, it is also a measure of the upwelling and wintertime mixing strength [*Anderson et al.*, 2009; *Jaccard et al.*, 2013]. Additionally, eolian dust (and Fe) input was reconstructed to detect its stimulating effect on productivity. Deep ocean ventilation was reconstructed by the oxygenation state of deep ocean water masses, which is a combination of the initial O_2-content in surface water and the amount of O_2 consumed by remineralization of organic matter in the ocean interior. The oxygenation state can be inferred from redox-sensitive trace metals, which behave differently under specific redox conditions [*Tribovillard et al.*, 2006]. The most meaningful trace metals were measured, including authigenic uranium (aU), manganese (Mn), molybdenum (Mo) and vanadium (V). Further details about the study site and the individual analytical techniques including measurement uncertainties will be outlined in the Material and methods chapter.

2.8. Research questions

The goal of this study was to expand the spatial and temporal coverage of BEP fluxes and

deep water ventilation/oxygenation in the Pacific sector of the SO. Likewise, well known events and characteristic transitions that occurred during the last glacial period should be identified thanks to the high-resolution proxy records. The multi-proxy approach helps to constrain the efficiency of the biological pump in this region. Thus by reconstructing BEP, nutrient conditions and deep ocean ventilation, past ocean's leverage on pCO_{2atm} in the SW Pacific should be identified, which could help to predict future oceanic changes under ongoing warming of the climate. With the sedimentary data from this study and the inclusion of previously measured proxies on core SO136-111, as well as data from other archives, the following research questions should be answered.

- Does core SO136-111 show glacial-interglacial changes in BEP fluxes (bioBa, Opal, $CaCO_3$), which can be linked to variable pCO_{2atm}?
- Is it possible to infer qualitative changes about the deep ocean O_2 content from redox-sensitive trace metals and are they correlated do BEP fluxes?
- Are there millennial scale events, such as the Antarctic warming events, recorded in the proxy records of BEP?
- Is there an enhanced dust (Fe) input during glacial stages and what are the implications on BEP and nutrient consumption?
- How is $CaCO_3$ export/preservation related to carbonate chemistry changes in the deep and surface ocean?

This master thesis has been part of the master program "Climate Sciences" at the Oeschger Centre, University of Bern, Switzerland. It was performed within the research group "Paleoceanography and marine biogeochemistry" at the Institute of Geological Sciences, University of Bern, where sample preparation and most measurements were conducted.

3. Material and methods

Gravity core SO136-111 (56°40'S, 160°14'E) was retrieved from the southern Emerald Basin during the TASQWA cruise with the German research vessel Sonne in 1998 (Fig. 6). The core was retrieved from a water depth of 3912 meters, currently bathed by LCDW, which mainly consists of southern sourced deep waters and eastward flowing NADW. The sediment is predominantly composed of siliceous ooze. In addition, fluctuating fractions of lithogenic and calcareous material are present [*Thiede et al.*, 1999]. The core site is at the location of the modern APF, lacking seasonal sea-ice coverage during the Holocene. However, during the coldest periods of the two last glacial cycles, seasonal sea ice was present for about 2 months during wintertime [*Crosta et al.*, 2004]. Today surface water is enriched in macronutrients (silicate, phosphate, nitrate) compared to regions further to the north, where nutrients are rapidly consumed. Deep waters are nutrient-rich and relatively well ventilated, with oxygen concentrations around 200 µmol/kg [*Bostock et al.*, 2013]. The core location from a SO perspective and in a cross section throughout the major water masses is depicted in Fig. 6.

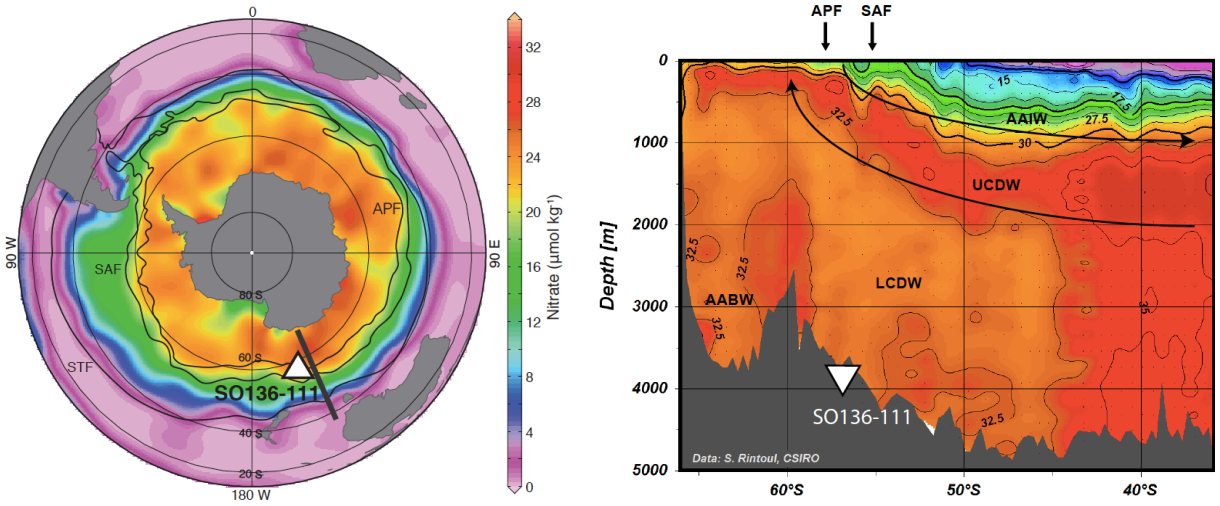

Fig. 6. Location of core SO136-111. The figure on the left indicates the strong gradient in annual surface nitrate concentration within the SO. The thin black lines indicate the positions of the modern APF, SAF and STF. The thick black line on the left illustrates the cross section illustrated in the right Figure. SO136-111 is located at the modern position of the APF and bathed by LCDW (modified after Schlitzer, 2000).

3.1. Sedimentary data

The discrete sediment samples were collected at the core repository at the GEOMAR in Kiel, Germany. In total 155 samples were collected, down to a core depth of 527 cm, covering the last glacial cycle. Up to 172 cm (approximately the MIS[5] 4/5 transition) a sample resolution of 2 cm, if applicable, was chosen, whereas older samples were collected every 5 cm. This should allow detecting millennial scale events in more recent times and broader glacial-interglacial variations over the entire section. Samples were then freeze-dried under vacuum pressure of 4 mbar and at a temperature of -50 °C during 4 days at the Institute of Plant Sciences, University of Bern. The dry sediments were homogenized with a pestle and stored for further preparation. In the following the different methods for the proxy measurements are briefly described, although the individual proxies with its uncertainties and limitations are discussed further below.

3.1.1. Uranium-thorium measurements using ICP-MS

The combined measurement of U and Th isotopes (^{238}U, ^{234}U, ^{232}Th and ^{230}Th) allows to constrain the vertical flux of individual sedimentary constituents, by calculating the excess/deficit of ^{230}Th over a given time interval [*Francois et al.*, 2004]. Additionally, the lithogenic fraction in the sediment can be inferred from ^{232}Th, and the accumulation of authigenic U (aU) is calculated by its excess over the detrital input. Measurements were performed on a multi-collector inductively coupled plasma mass spectrometer (ICP-MS) at the Institute of Geological Sciences, University of Bern. Briefly, 0.2 g sample material was

[5] Marine isotope stages (MIS) are time periods, classified according to the δ^{18}O-signal in marine sediment records, with even numbers representing glacial stages. In the last glacial cycle MIS 2 and 4 are the two cold stages. Additionally, MIS 5 is subdivided into 5a-5e, with MIS 5e as the warmest substage and a possible analog for the Holocene. [*Lisiecki and Raymo*, 2005]

spiked and completely digested in an acid cocktail including concentrated HNO_3, HCl and HF. The mixture was heated under pressure for 90 min to a maximum of 180°C, and afterwards evaporated at a maximum temperature of 110°C. The Th fraction was separated from U by column chromatography using an ion exchange resin, so that isotopes of the two elements could be measured individually. The detailed procedure of the microwave digestion, element separation and measurement setup with some modifications is described elsewhere, [*Bernsdorff*, 2008]. For the purpose of quality control, every batch run included a blank and a standard (Urem). A double spike ($^{233}U/^{236}U$) for U and a single spike (^{229}Th) for Th was used to determine the sample isotope concentration (for the calculation see Appendix). The error of analytical precision was generally lower than 1%. Internal and external reproducibility was on average 1.2% and 2.5%, respectively. However, due to the average deviation of the Urem-standard values, a general error of 3.9% was added to each sample.

3.1.2. Opal and $CaCO_3$ measured by Fourier transform infrared spectroscopy (FTIRS)

The detailed FTIRS procedure with the measurement setup and development of a calibration set is described elsewhere [*Vogel et al.*, in prep.; *Rosen et al.*, 2011; *Meyer-Jacob et al.*, 2014]. FTIRS relies on the absorption spectra of individual molecular bindings, such as Si-O in opal and C-O in $CaCO_3$. From the absorption spectra, individual sediment components can be determined. 11 mg sample was mixed with 500 mg potassium bromide (KBr). The mixture was homogenized and dried to avoid water adsorbing to the samples, which appeared to be a problem in the first opal results owing to a modified absorption spectra. The calibration set for carbonate has not been completed, wherefore FTIRS derived $CaCO_3$ content was recalibrated with coulometric derived inorganic carbon concentration, measured in the same core [*Sturm*, 2003]. For opal, most samples were measured at least twice with an overall internal reproducibility better than 6%. External verification with conventionally measured opal content at the University of British Columbia (UBC), Vancouver, Canada, resulted in an R^2 of 0.90 (see Appendix).

3.1.3. Major and minor elements using ICP-MS

Measurement of the major elements Fe, Al, and trace metals Ba, Mn, Mo and V was conducted at Activation Laboratories (Actlabs), Ontario, Canada. Digestion of 0.25 g sediment was achieved by heating the samples in nitric and perchloric acid. The digestion procedure was repeated to ensure total digestion. Measurements were performed by ICP-MS, with an overall reproducibility based on sample replicates and standards better than 3%, yet for Mo it was above 10% due to the very low concentrations in samples.

3.1.4. Age model

In previous studies the age model of core SO136-11 was constructed by aligning $\delta^{18}O$ of the planktonic foraminifera species N. pachyderma to the benthic $\delta^{18}O$ SPECMAP stack assuming no phase lag. Age tie points were supported by radiocarbon dates on planktonic foraminifera shells back to 43 kyr BP [*Sturm*, 2003; *Crosta et al.*, 2004]. Since this age model

was constructed with an older reference curve and considering the general uncertainties related to the planktonic-benthic correlation, the existing age model was updated. The new age model, following the approach outlined in [*Studer et al.*, 2015], is based on the assumption that the planktonic $\delta^{18}O$ signal from SO136-111 closely follows Antarctic temperature variations, recorded by the deuterium ratio (δD) in ice cores [*Jouzel et al.*, 2007]. In addition, three radiocarbon dates were included (Fig. 7). The graphical correlation between the $\delta^{18}O$ values of N. pachyderma and EDC δD was performed using AnalySeries [*Paillard et al.*, 1996]. The final result (see Fig. 7) shows good agreement with the initial age model, however, a deviation of about 2 kyr at terminations I, and 5 kyr at termination II, and in particular during MIS 5 occurred. The uncertainties in the age model do not allow evaluating lead-lag relations to other records, but should not affect the general interpretations. Sedimentation rate and exact tie points are included in the Appendix.

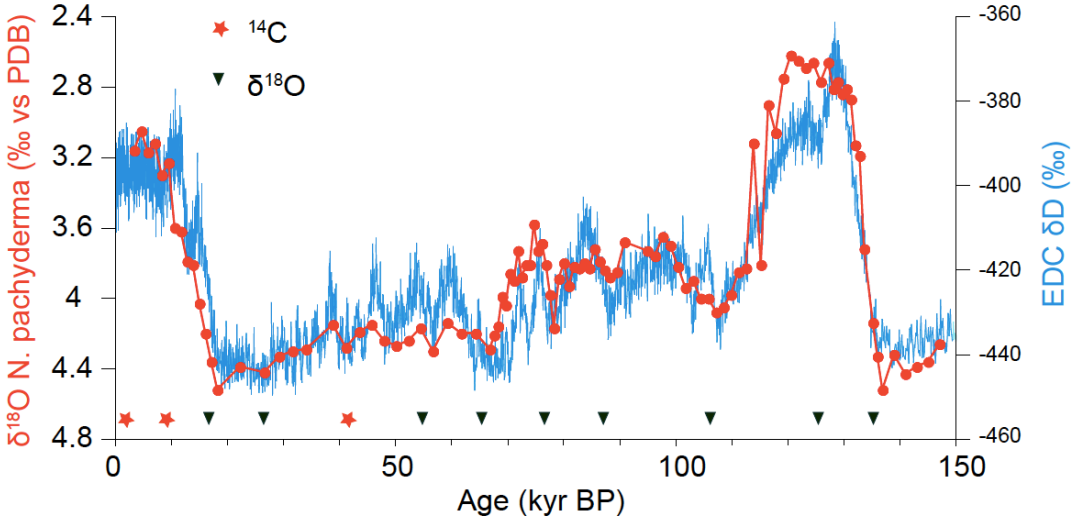

Fig. 7. Modified age model from the correlation of planktonic $\delta^{18}O$ and EDC δD. Planktonic $\delta^{18}O$ values of N. pachyderma are from [*Sturm*, 2003], radiocarbon dates (red stars) are from [*Crosta et al.*, 2004] and EPICA Dome C deuterium ratio (EDC δD) is from [*Jouzel et al.*, 2007]. Tie points to adjust the two records are indicated by the black triangles on the bottom.

4. Proxies

In this chapter the individual proxy records including their uncertainties and limitations are discussed. As mentioned above, it is more reliable to interpret a combination of different proxies that express the same variable. To reconstruct BEP and by inference C_{org} export, fluxes of opal, bioBa and possibly $CaCO_3$ together represent a useful measure. The redox state at the sediment-water interface was determined using a combination of redox-sensitive trace metals precipitated from the water column (Mn, V, Mo) or formed within the sediment (aU). With this approach, variable sedimentary preservation and other peculiarities of single proxy records can be circumvented [*Frank et al.*, 2000].

4.1. ^{230}Th normalization

Sediment redistribution on the ocean floor has been shown to significantly modify sediment mass accumulation patterns [*Francois et al.*, 1993]. In particular in the SO, strong bottom

currents are responsible for syndepositional redistribution sediments [*Frank et al.*, 2000]. It is thus necessary to correct the lateral sediment input, so that only vertical rain rates can be considered. *Bacon* [1984] proposed that the scavenging rate of ^{230}Th is equal to its known production rate (β_{230}) from the decay of ^{234}U in the water column. Any excess in the sedimentary ^{230}Th inventory was supplied laterally and indicates sediment focusing. In contrast to ^{234}U, ^{230}Th is a very particle reactive isotope and is rapidly scavenged from seawater by adsorption onto sinking particles. Assuming that scavenged ^{230}Th is equal to its production in the water column, an inverse relationship between the preserved vertical flux rate F(^{230}Th) (g/cm^2/kyr) and the activity[6] of [$^{230}Th_{ex,0}$] can be inferred by:

$$F(^{230}Th) = \frac{\beta_{230} * z}{[^{230}Th_{ex,0}]} \quad \text{(Eq.3)}$$

where β_{230} = 2.67*10^{-5} dpm/cm^3/kyr, z = water depth in cm and [$^{230}Th_{ex,0}$] = ^{230}Th decay corrected activity after subtracting the detrital and authigenic fraction [*Francois et al.*, 2004]. The measured [$^{230}Th_{meas}$] consists of three different sources; (i) the scavenged fraction [$^{230}Th_{ex}$], which is of interest to quantify the vertical flux, (ii) the detrital fraction [$^{230}Th_{det}$], (iii) and finally the authigenic fraction [$^{230}Th_{aut}$] related to the incorporation of U into the sediment under reducing conditions (see below) [*Francois et al.*, 2004].

The detrital fraction can be inferred by assuming secular equilibrium between [$^{230}Th_{det}$] and [$^{238}U_{det}$], and a constant [$^{238}U_{det}$]/[$^{232}Th_{det}$] ratio of 0.4 ± 0.1 for the SO [*Henderson and Anderson*, 2003]. Here, 0.43 is the lowest value of all measured [^{238}U]/[^{232}Th] ratios, and is assumed to illustrate conditions devoid of U ingrowth, and thus represents a reasonable approximation for the detrital ratio. [$^{230}Th_{det}$] is thus given by:

$$[^{230}Th_{det}] = [^{238}U_{det}] * \alpha = 0.43 * [^{232}Th_{det}] * \alpha \quad \text{(Eq. 4)}$$

where [$^{232}Th_{det}$] is equal to the measured [$^{232}Th_{meas}$] as this isotope is almost exclusively of detrital origin [*Francois et al.*, 2004]. The factor α = 0.96 takes the alpha-recoil into account, in that [$^{230}Th_{det}$] is not exactly in secular equilibrium with [$^{238}U_{det}$] but slightly lower [*Bourne et al.*, 2012].

[$^{230}Th_{aut}$] is provided by [$^{238}U_{aut}$] = [$^{238}U_{meas}$] - [$^{238}U_{det}$]. As [$^{230}Th_{aut}$] is produced from decaying [$^{234}U_{aut}$] and average seawater ratio of [^{234}U]/[^{238}U] is 1.147 [*Bourne et al.*, 2012], [$^{230}Th_{aut}$] is given by:

$$[^{230}Th_{aut}] = 1.147 * [^{238}U_{aut}] * \left(1 - e^{-\left(\frac{\ln 2 * t}{75.7}\right)}\right) \quad \text{(Eq. 5)}$$

where t is the time since deposition and 75.7 is the half-life of ^{230}Th in kyrs [*Francois et al.*, 2004]. It is now possible to calculate [$^{230}Th_{ex}$] from the measured (total) ^{230}Th activity [$^{230}Th_{meas}$]:

$$[^{230}Th_{ex}] = [^{230}Th_{meas}] - [^{230}Th_{det}] - [^{230}Th_{aut}] \quad \text{(Eq. 6)}$$

Since [$^{230}Th_{ex}$] denotes the activity at present times and the initial scavenged ^{230}Th activity [$^{230}Th_{ex,0}$] at the time of deposition is of interest, it is necessary to correct for this decay, which is shown in Eq. 7 [*Francois et al.*, 2004].

[6] Activity unit is dpm/g written as [^{230}Th], (dpm = disintegrations per minute)

$$\left[^{230}Th_{ex,0}\right] = \left[^{230}Th_{ex}\right] * e^{\left(\frac{\ln 2 * t}{75.7}\right)} \quad \text{(Eq. 7)}$$

To calculate the vertical flux, the result of Eq. 7 is inserted into Eq. 3. All reported export production proxies in this study are normalized by ^{230}Th; concretely the weight percentage of the respective sedimentary component is multiplied by F(^{230}Th) from Eq. 3. Uncertainties for the presented flux calculations arise from the assumed detrital ratio and age model uncertainties, which can lead to both over- or underestimation of the vertical flux [*Bourne et al.*, 2012]. An additional limitation of this flux calculation is that it represents only the preserved vertical flux rate, because post-depositional degradation of particles increases [$^{230}Th_{ex,0}$] in the sediment, whereby F(^{230}Th) declines. Sediment redistribution over different water depths also leads to calculation errors, because the ^{230}Th production rate depends on the water depth above the sediment core. Likewise the assumed immediate scavenging of ^{230}Th has been questioned, although this is of more importance in very high or very low particle flux regions [*Francois et al.*, 2004]. At core site SO136-111, age model uncertainties are possibly the largest source of error, because [$^{230}Th_{det}$] and [$^{230}Th_{aut}$] are much smaller than [$^{230}Th_{ex}$].

4.2. Opal

Diatoms and radiolarians build their frustules with opal (biogenic silica) from dissolved silicic acid in the surface ocean [*Bradtmiller et al.*, 2010]. Opal production in the modern surface ocean is mainly limited by the availability of silicic acid; consequently, in the SO, the nutrient supply from below controls its production. Spatio-temporal changes in the export flux of opal were proposed to reflect variable upwelling patterns around the APF and in the AZ [*Anderson et al.*, 2009]. The export of opal and by inference C_{org}, is related to BEP, however, undersaturation of seawater with respect to biogenic silica affects the preservation efficiency of opal shells both in the water-column and within the sediment. Due to this variable preservation (preservation is enhanced, if sediment accumulation rate is high) the accumulation rate in sediments is non-linearly linked to opal production in the surface ocean [*Frank et al.*, 2000]. Likewise a variable C_{org}:opal ratio in the sinking particles complicates the assessment of opal for BEP [*Kumar et al.*, 1995]. Considering several independent BEP proxies together can separate preservation versus production driven changes in the opal record. Another possibility is to include ^{231}Pa/^{230}Th ratio, which varies in concert with opal flux, as ^{231}Pa is preferentially scavenged by opal particles, and once deposited, ^{231}Pa/^{230}Th is not affected by dissolution [*Bradtmiller et al.*, 2009].

4.3. Biogenic barium

Biogenic barium (bioBa) is a proxy for the integrated export of organic matter to the sediment [*Dymond et al.*, 1992]. As sinking organic matter is decomposed in the water column, barite crystals ($BaSO_4$) form in microenvironments with dissolved Ba and supersaturated sulfate (SO_4) concentrations [*Francois et al.*, 1995; *Ganeshram et al.*, 2003]. Under strongly reducing conditions, SO_4 reduction alters the preservation of $BaSO_4$ and thus bioBa can be compromised as a suitable, reliable proxy for paleoproductivity estimates [*Dymond et al.*, 1992]. However, under oxic/suboxic conditions, typical for open-ocean conditions, $BaSO_4$

preservation is not significantly affected by SO_4 reduction. BioBa is the excess fraction of Ba in the sediment; it is derived from the measured (total) Ba concentration corrected for the detrital background:

$$bioBa(\%) = Ba - Al * \left(\frac{Ba}{Al}\right)_{det} \quad \text{(Eq. 8)}$$

with $(Ba/Al)_{det}$ = 0.0068 representing the average upper continental crust ratio [*Taylor and McLennan*, 1995]. The assumption of a constant and known detrital ratio over time can be an important shortcoming of this proxy, as this ratio could change over time. However, combined with opal fluxes, bioBa can be a robust measure for BEP.

4.4. $CaCO_3$

The formation of $CaCO_3$ in the surface ocean is driven mainly by coccolithophores, foraminifera and pteropods [*Salter et al.*, 2014]. $CaCO_3$ accumulation rates in sediments are not always suitable to reconstruct BEP, as $CaCO_3$ preservation is strongly affected by ocean ALK and in turn by the depth of the lysocline. The core depth (3912 m) is in particular influenced by shoaling/deepening of the lysocline over glacial-interglacial cycles, as today the lysocline is approximately at 3600 m [*Sturm*, 2003]. Hence, instead of providing information related to BEP, the carbonate flux helps to constrain the preservation of $CaCO_3$ in the deep ocean, especially if rapid transitions in $CaCO_3$ are observed which could indicate a transient deepening/shoaling of the lysocline [*Jaccard et al.*, 2013].

4.5. Redox-sensitive trace metals

The redox conditions of deep ocean waters and/or pore water in sediments are a function of the initial oxygen content and subsequent remineralization of C_{org}. There is a variety of redox-sensitive trace metals, which can be used to infer the redox-state in the water mass or at the sediment interface. Here, the focus lies on Mn, aU, Mo and V, as the combination of those elements allows to differentiate between oxic, suboxic, anoxic or euxinic conditions, respectively [*Tribovillard et al.*, 2006]. Each redox-sensitive trace metal only accumulates under certain redox conditions. To infer the flux variations to the sediment driven by redox state changes, trace elements (Mn, Mo, V) concentrations are normalized to the average crustal ratio relative to aluminum (Al) [*Taylor and McLennan*, 1995]. The accumulation of aU was inferred from the excess of ^{238}U over ^{232}Th, as ^{232}Th originates exclusively from a detrital source and ^{238}U is of both detrital and/or authigenic origin [*Francois et al.*, 2004]. Thus aU is given by:

$$aU(ppm) = ([^{238}U_{meas}] - 0.43 * [^{232}Th_{det}]) * \frac{1}{\eta} \quad \text{(Eq. 9)}$$

with η = 0.746 as a conversion factor (1 ppm = 0.746 dpm/g) and 0.43 is the assumed $[^{238}U_{det}]/ [^{232}Th_{det}]$ ratio (see above). Normalization allows to reconstruct the excess of each redox-sensitive trace metal, however, this requires again the assumption of a constant average crustal ratio, which together with ambiguous inferences for redox-sensitivity, represents a general limitation of this method [*Tribovillard et al.*, 2006].

Enrichment of Mn is associated with the oxidation of soluble Mn(II) into insoluble Mn(III)

and Mn(IV) species, which are precipitated as Mn-oxides. Thus excess Mn (above the detrital ratio) is associated with well oxygenated (oxic) water masses [*Jaccard et al.*, 2009]. In addition, the precipitation of Mn-oxides influence other redox-sensitive trace metals, by transferring them to the sediment [*Tribovillard et al.*, 2006]. In contrast, Mo is either enriched under anoxic conditions by reducing the soluble Mo(IV) to insoluble Mo species, or through the association with Mn-oxides under oxic conditions. Under suboxic conditions, however, little or no excess Mo is expected [*Jaccard et al.*, 2009]. V behaves very similarly to Mo, and is precipitated under reducing conditions and can also be associated with Mn-oxides [*Tribovillard et al.*, 2006]. Finally aU is accumulated under reducing conditions within the sediment layer. In oxygenated waters U(VI) is homogeneously distributed, however, in sediment pore waters U(VI) is reduced under suboxic conditions to U(IV), whereby diffusion of U into the sediments leads to the accumulation of aU [*Bradtmiller et al.*, 2010]. Hence, the concentration of aU is a function of bottom water oxygenation and the flux of C_{org} to the sediment. A higher C_{org} flux and consequently enhanced remineralization within the sediment increases aU concentrations. Likewise, low bottom water oxygenation promotes aU to accumulate. The proxy is complicated by post-depositional removal of aU (including Mo and V), which can occur from increased bottom water oxygenation and a deepening of the redoxcline after initial deposition. This process leads to the dissolution of previously precipitated aU and leads to a characteristic accumulation peak at the redoxcline. Additionally, aU accumulation does not enable to distinguish between laterally and vertically supplied sediment components [*Frank et al.*, 2000]. Therefore it is preferentially present in sediments with high mass accumulation rates. As aU is not scavenged out of the water column, the accumulation of aU is a concentration measure and not a flux estimate.

4.6. Lithogenic content

As ^{232}Th is solely present in detrital material, this isotope represents a reliable measure of the lithogenic material in the sediment. Assuming a constant detrital ^{232}Th concentration of 10.7 ppm [*Taylor and McLennan*, 1995], the lithogenic flux is provided by:

$$litho.Flux\left(\frac{g}{cm^2 * kyr}\right) = [^{232}Th_{det}] * \frac{\mathbf{1}}{\gamma * 10.7} * F(^{230}Th) \qquad \text{(Eq. 10)}$$

with γ = 0.243 as a conversion factor (1ppm = 0.243 dpm/g) [*Chase et al.*, 2003]. The assumption of the average crustal ^{232}Th concentration of 10.7 ppm bears some uncertainty, however globally the range (10 – 14 ppm) in the upper continental crust is relatively narrow [*Taylor and McLennan*, 1985]. Even if the ratio was different from 10.7 ppm yet constant over time, this would only affect the absolute flux values, however, the relative variations in lithogenic fluxes over glacial cycles would be the same [*Anderson et al.*, 2014]. Fe is of more interest than the total lithic flux itself, when assessing the implications on biological productivity, which is why Fe concentrations were measured individually. Yet as Fe cycling is part of the marine biological cycle and supply to the Antarctic Zone is dominated from below [*Martínez-Garcia et al.*, 2011], considering Fe fluxes together with the lithogenic flux is a more accurate measure of lithogenic Fe supply.

5. Results

5.1. Biological export production

Downcore reconstructions of $CaCO_3$, biogenic opal and bioBa export fluxes in comparison to pCO_{2atm} are shown in Fig. 8. On top, the planktonic $\delta^{18}O$ record of N. pachyderma allows to distinguish MIS stages, with blue vertical bars highlighting cold periods (MIS 2, 4 and 6). The strong coherency between opal and bioBa over the last 150 kyr supports the notion that diatoms dominate organic carbon export in the SO [*Frank et al.*, 2000; *Bradtmiller et al.*, 2009]. Following the reasoning outlined by *Anderson et al.* [2014], the similarities between both records reflect changes in surface biological productivity rather than variable preservation of opal and barite, which depends on different biochemical conditions [*Jaccard et al.*, 2009]. Additional support for productivity driven changes results from the covariance of opal accumulation and $^{231}Pa/^{230}Th$ ratio, measured at nearby core E27-23 (59°64'S, 155°24'E) [*Anderson et al.*, 2009]. Both, opal and bioBa show a strong climate-related signal with generally higher export production during warmer periods (MIS 1 and 5) and decreasing BEP during cold stages, characteristic for AZ productivity pattern over glacial-interglacial cycles [*Chase et al.*, 2003; *Jaccard et al.*, 2013]. In fact, the opal flux almost approaches zero during peak glacial MIS 2, 4 and 6. However, around 140 kyr BP relatively high opal and especially high bioBa fluxes (1 mg/cm^2/kyr) are observed. Terminations (Term) I and II are accompanied by an increase in BEP, although the largest fluxes, in particular those for opal, are found during MIS 5a – 5c with values approaching 0.8 g/cm^2/kyr, consistent with other records from the central Pacific AZ [*Studer et al.*, 2015] and the Atlantic AZ [*Jaccard et al.*, 2013]. These records, however, reveal high opal accumulation during MIS 5e. Compared to these cores, opal fluxes at SO136-111 are significantly lower over the entire time period. Contrasting the opal record with nearby cores show similar opal fluxes at the LGM, whereas cores further to the south indicate a stronger deglacial rise and higher Holocene opal fluxes, consistent with the modern opal productivity maximum located south of core site SO136-111 [*Bradtmiller et al.*, 2009]. Likewise bioBa fluxes are of similar magnitude in nearby sediment cores [*Chase et al.*, 2003], but significantly lower than in the Atlantic AZ [*Jaccard et al.*, 2013] and the Pacific SAZ [*Lamy et al.*, 2014]. The most striking feature is the distinct drop in pCO_{2atm} at the MIS 4/5 transition coinciding with a sharp decrease in opal (from 0.8 to <0.1 g/cm^2/kyr) and bioBa fluxes. This is consistent with drastic reduction in opal accumulation and low Ba/Fe (indicating low Ba excess) ratios after 70 kyr BP in the central Pacific AZ [*Studer et al.*, 2015]. Furthermore a strong coupling of opal, bioBa and pCO_{2atm} during MIS 2-4 is observed, in particular during the millennial-scale fluctuations characteristic of MIS 3 (see also Fig. 9). The correlation coefficient between opal fluxes and pCO_{2atm} over the entire record is not very large, yet between the last deglaciation and MIS 5b a high $R^2 = 0.74$ has been inferred.

The aforementioned complication of $CaCO_3$ owing to strong dissolution changes does not allow making inferences about past productivity changes. $CaCO_3$ accumulation was fairly constant over most of the last glacial period, fluctuating around 0.2 g/cm^2/kyr. Yet rapid, transient increases centered around Term I and II coincide with the deglacial rise in pCO_{2atm} (Fig. 8). Such transient deglacial $CaCO_3$ peaks have been observed in the Atlantic AZ over multiple glacial cycles [*Jaccard et al.*, 2013].

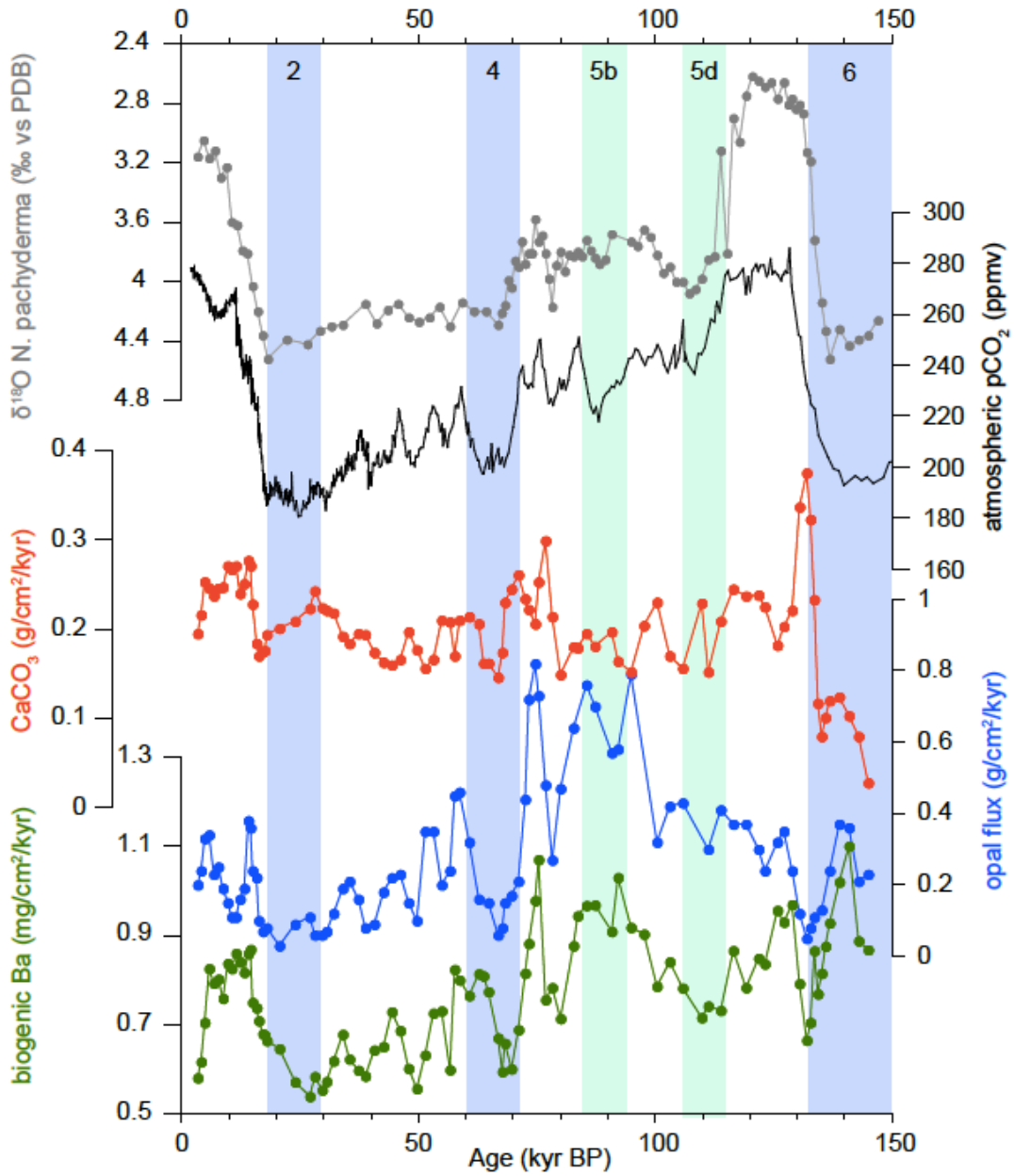

Fig. 8. Multi-proxy records ($CaCO_3$, opal, bioBa) from core SO136-111 covering the last glacial cycle. Additionally, pCO_{2atm} from a recent ice core composite [*Bereiter et al.*, 2015] and planktonic (N. pachyderma) $\delta^{18}O$ data [*Sturm*, 2003] are shown on top. All fluxes of BEP are constrained by ^{230}Th normalization. Blue columns represent glacial marine isotope stages (MIS) 2, 4 and 6, as well as substages 5b and 5d (turquois columns).

The strong coupling between Antarctic temperatures [*Jouzel et al.*, 2007], and pCO_{2atm} [*Bereiter et al.*, 2015] is illustrated in Fig. 9. *Fischer et al.* [2010] noted a correlation coefficient of 0.84 for EDC δD and pCO_{2atm}. Since opal flux of SO136-111 is frequently correlated to pCO_{2atm}, this finding also holds true for opal and δD, with deviations at Term II and during MIS 5e (discussed later). The rest of the opal record shows a remarkably high coherency to Antarctic temperature, again in particular between MIS 2-4. During this period rising Antarctic temperatures coincide with higher levels of pCO_{2atm} and increasing opal flux a pattern previously noted in the Atlantic SO [*Anderson et al.*, 2009]. From the δD record it becomes clear, that a large fraction of the cooling into glacial temperatures already occurred at the MIS 5d/5e boundary and then again into the glacial MIS 4, where opal productivity declines simultaneously. At the bottom of Fig. 9, the duration of sea ice coverage in months

per year at core site SO136-111 is depicted. Reconstructions are based on diatom assemblages and the individual species affinity to ocean waters with or without sea ice presence [*Crosta et al.*, 2004]. During glacial periods, sea ice was present, albeit only during a short period (max. 2 months) in austral winter. Sea ice coverage is strongly coupled to Antarctic temperatures and responds quickly to temperature variations (Fig. 9). As sea ice is only present during winter months, it does not directly affect opal productivity.

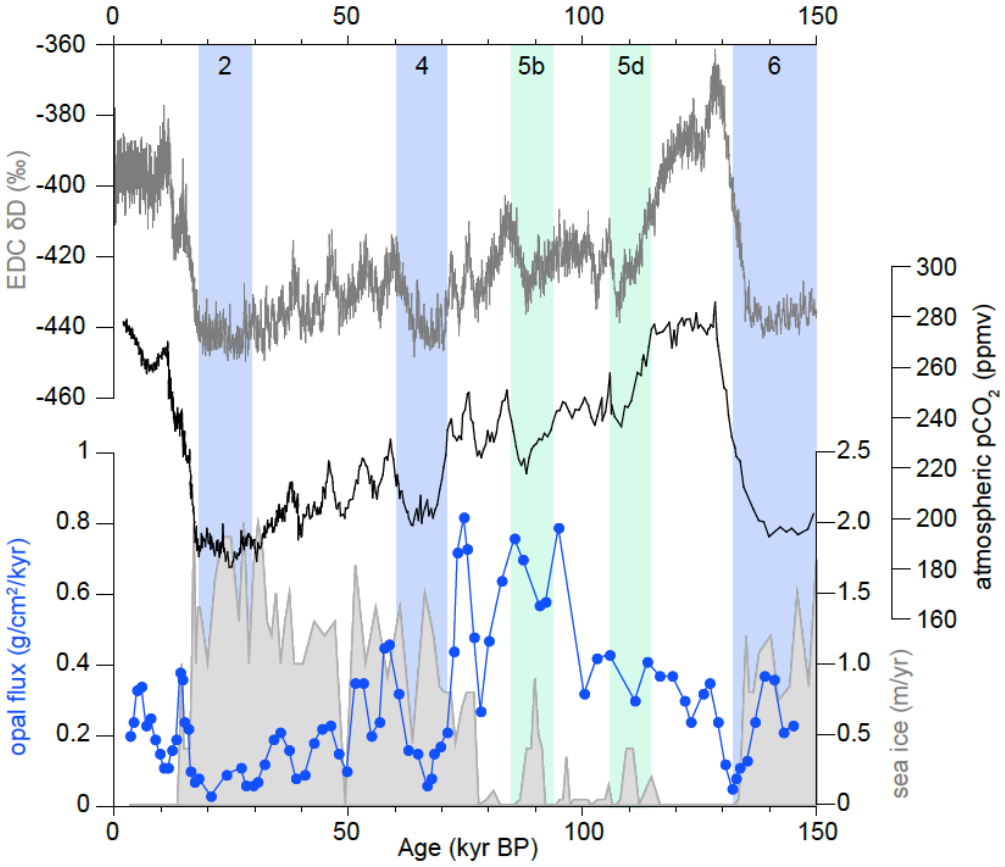

Fig. 9. Antarctic conditions as recorded over the last glacial cycle. Temperatures inferred by deuterium ratio (δD) from ice core EPICA Dome C (EDC) [*Jouzel et al.*, 2007], pCO_{2atm} composite [*Bereiter et al.*, 2015], and opal flux (this study). Grey shaded area indicates past sea-ice coverage in months per year (m/y) reconstructed by diatom assemblages [*Crosta et al.*, 2004].

5.2. Redox conditions

Modern oceanographic conditions indicate that core site SO136-111 is bathed by LCDW, thereby holding relatively high oxygen concentrations of approximately 200 µmol/kg [*Schlitzer*, 2000]. Hence, sediment accumulation occurs under oxic conditions at present times. The high O_2 concentration is controlled by the input of well-ventilated southern sourced deep waters [*Bostock et al.*, 2013]. Considering the downcore record of redox-sensitive trace metals (Fig. 10), excess Mn reveals that oxic conditions persisted at the water-sediment interface throughout the past 150 kyr. Irrespective of the detrital ratio selected, Mn excess indicates precipitation of Mn-oxides from well-oxygenated bottom waters [*Jaccard et al.*, 2009]. At Term I and II, Mn/Al shows a distinct increase (note the logarithmic scale for Mn/Al). Another striking feature is the two order of magnitude enrichment after 100 kyr BP, which coincides with the highest opal export flux (see Fig. 9). Post-depositional dissolution in

reducing pore waters, could affect the vertical diffusion of Mn within the sediment [*Tribovillard et al.*, 2006], however, since Mn enrichment is consistently preserved, this process does not prohibit Mn accumulation.

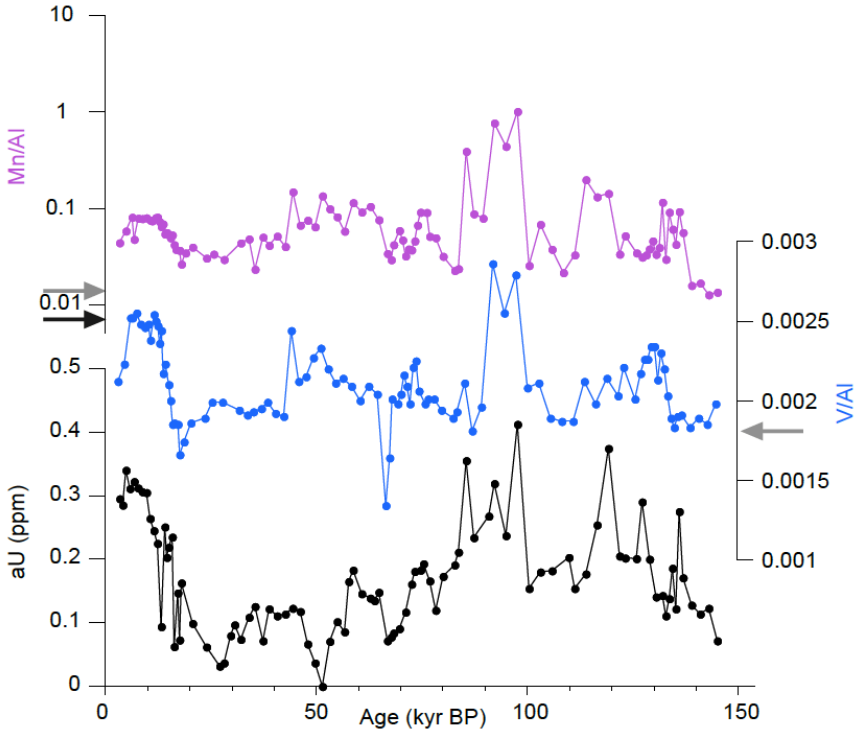

Fig. 10. Redox sensitive trace metals manganese (Mn), vanadium (V) and authigenic uranium (aU). Mn and V are normalized to aluminum (Al), whereby the excess over the average upper continental crust (AUCC) ratio can be inferred. Note the logarithmic scale for Mn/Al. AUCC ratio are Mn/Al = 0.0075 and V/Al = 0.00075, indicated by the black arrow for Mn/Al (AUCC for V/Al is outside the scale). In addition the grey arrows indicate average andesitic crust ratio (Mn/Al = 0.0116 and V/Al = 0.0018 [*Taylor and McLennan*, 1995]. Accumulation of aU, given in ppm, has been calculated with a detrital $^{238}U/^{232}Th$ ratio of 0.43, consistent with the proposed 0.4 (± 0.1) ratio for the SO [*Henderson and Anderson*, 2003].

Excess V determined from V/Al ratio higher than in the AUCC (V/Al = 0.00075) and AAC (V/Al = 0.0018) [*Taylor and McLennan*, 1995] potentially violate the observation of oxic waters, since V is accumulated under reducing (suboxic-euxinic) conditions (Fig. 10). Yet, the strong coupling between V and Mn in the sediment record rather indicates that V accumulation is coupled to Mn-oxides. It was previously noted that Mn cycling is important for other redox-sensitive trace metals, since the sedimentary emplacement is catalyzed by Mn-oxides [*Tribovillard et al.*, 2006]. After deposition, mildly reducing pore waters promote V enrichment. Mo data (not shown) suggests no excess above the detrital background, however, due to the larger measurement uncertainties for this element it is not further considered. Similar to V enrichment, the presence of aU indicates mildly reducing conditions in some intervals. The aU record shows similar variations as Mn/Al and V/Al (Fig. 10), yet a much closer relationship to bioBa flux is revealed, when comparing these two records (Fig. 11).

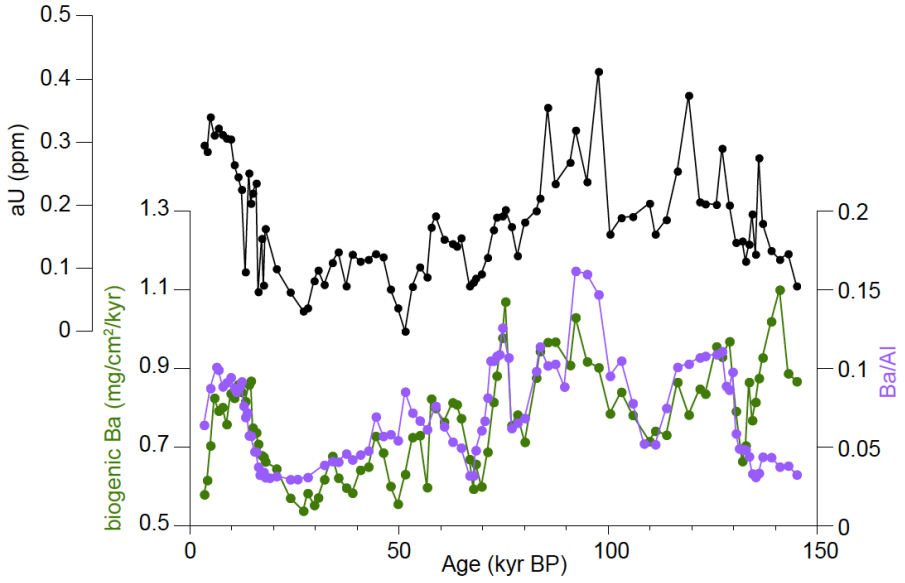

Fig. 11. Comparison of authigenic uranium (aU) and biogenic barium. In addition to the biogenic barium (bioBa) flux the Ba/Al ratio is shown, which deviates from the bioBa flux during MIS 6. For calculation of bioBa and aU see chapter Material and methods.

The coupling of C_{org} and aU has been noted in various other regions [*Chase et al.*, 2001; *Martínez-Garcia et al.*, 2009] of the SO. Since aU deposition occurs within the sediment layer, where pore water redox state is influenced by both bottom water oxygenation and C_{org} remineralization, the presence of aU could reflect changes in both parameters [*Chase et al.*, 2003], yet based on the strong coherency of bioBa and aU it seems likely that biological productivity (and organic matter respiration) was the main driver of aU variations. Additionally, the contemporary Mn enrichment does not support low O_2 waters. At SO136-111 aU concentrations are very small (<0.4 ppm), consistent with other cores from the SW Pacific [*Chase et al.*, 2003]. The deglacial rise of aU at Term I and II in concert with increasing BEP contrasts the finding of previous studies from the Atlantic and Indian sectors of the SO showing distinct aU peaks at glacial maxima with aU concentrations up to 4 ppm [*Francois et al.*, 1997; *Frank et al.*, 2000; *Chase et al.*, 2001]. However, as aU in core SO136-111 is generally low, the record is sensitive to the assumed detrital $^{238}U/^{232}Th$ ratio, as a slight increase would drive aU to near-zero values. Furthermore, aU is formed within the sediment and thus cannot be normalized by ^{230}Th, wherefore it is vulnerable to sediment redistribution. Considering the redox sensitive trace metal records together suggests the presence of oxic waters indicated by excess Mn, whereas C_{org} remineralization within the sediment caused partially suboxic pore waters, which have lead to low aU concentrations in the sediment. The presence of oxic (suboxic) waters supports the use of bioBa as a paleoproductivity tracer, in that the prevailing O_2-availability prevents barite to be affected from SO_4 reduction, which would be the case under anoxic conditions [*Dymond et al.*, 1992].

5.3. Lithogenic fluxes and nutrient conditions

Enhanced lithogenic input to the SO have been reported from a variety of sediment records during ice ages [e.g., *Martínez-Garcia et al.*, 2009; *Anderson et al.*, 2014; *Lamy et al.*, 2014]. Similarly, Antarctic ice cores showed increasing eolian dust deposition (Fig. 12) [*Lambert et*

al., 2008]. In particular, the coldest intervals MIS 2, 4 and 6 reveal a substantial increase in dust loading over Antarctica and by inference the SO. The reconstruction of detrital input at core SO136-111 is consistent with this pattern with the highest detrital flux of up to 0.4 g/cm^2/kyr during the last two glacial maxima, as well as an increase during MIS 4. Since sea ice was partially present at core site SO136-111 (see Fig.9), ice-rafted debris (IRD) could be a possible contributor to the glacial increase in detrital input. However, the distinct coherency with EDC dust variations and a fairly consistent pattern throughout the Pacific SO sector supports a predominantly eolian origin of the detrital fraction [*Lamy et al.*, 2014]. Nevertheless, IRD might be relevant, which is further supported by the presence of dropstones found during the last termination [*Thiede et al.*, 1999] and the penultimate glacial maximum (this study). Due to the proximity of SO136-111 to the Australian dust source, deposition is larger compared to eastward regions from the SW Pacific [*Chase et al.*, 2003] and the central Pacific [*Lamy et al.*, 2014]. In addition to the total lithogenic flux, Fe supply is shown in Fig. 12. In contrast to ^{232}Th (which was used to calculate the lithogenic fraction, by assuming a detrital concentration of 10.7 ppm [*Taylor and McLennan*, 1995]), Fe is used by marine biology and is predominantly supplied to the AZ by upwelling waters [*Martínez-Garcia et al.*, 2011]. However, the strong covariance of both records, as well as with Antarctic dust concentrations, suggests increased eolian Fe supply during glacial times.

Enhanced Fe supply to the SAZ has been suggested as a major driver of more efficient biological productivity during glacial times [*Pollard et al.*, 2009; *Martínez-Garcia et al.*, 2011; *Jaccard et al.*, 2013]. Fe fluxes are compared with diatom-bound δ^{15}N values, a proxy for nitrate utilization previously measured at the same core [*Crosta and Shemesh*, 2002]. Although subsurface Fe supply might be of importance at core SO136-111, the data (Fig. 12) indicate a strong relationship between high δ^{15}N intervals (note the inverse ordinate scale) coinciding with periods of increased Fe supply. This is consistent with the higher resolved ODP 1090 record from the Atlantic Subantarctic, which actually shows similar sizes of Fe flux [*Martínez-García et al.*, 2014]. Alike to this study from the Atlantic SAZ, Fe fluxes of core SO136-111 started to rise during MIS 4 accompanied by higher δ^{15}N. However, it is also evident that during those periods opal (and bioBa) fluxes, which are assumed to be representative for BEP, are relatively low and even decrease with enhanced Fe supply (Figs.12 and 13). Thus at core site SO136-111 enhanced Fe supply during glacial stages did not promote higher BEP, similar to other cores from the AZ [*Frank et al.*, 2000; *Chase et al.*, 2003]. Again, the MIS 4/5 transition is noteworthy, where the previously mentioned distinct drop in opal flux is accompanied by enhanced Fe fluxes and nutrient consumption. Relatively low nutrient consumption has been inferred during deglacial transitions into MIS 5 and 1, respectively, co-occurring with higher opal fluxes. Opal and δ^{15}N evolution is in general consistent with a recent study from the central Pacific AZ [*Studer et al.*, 2015].

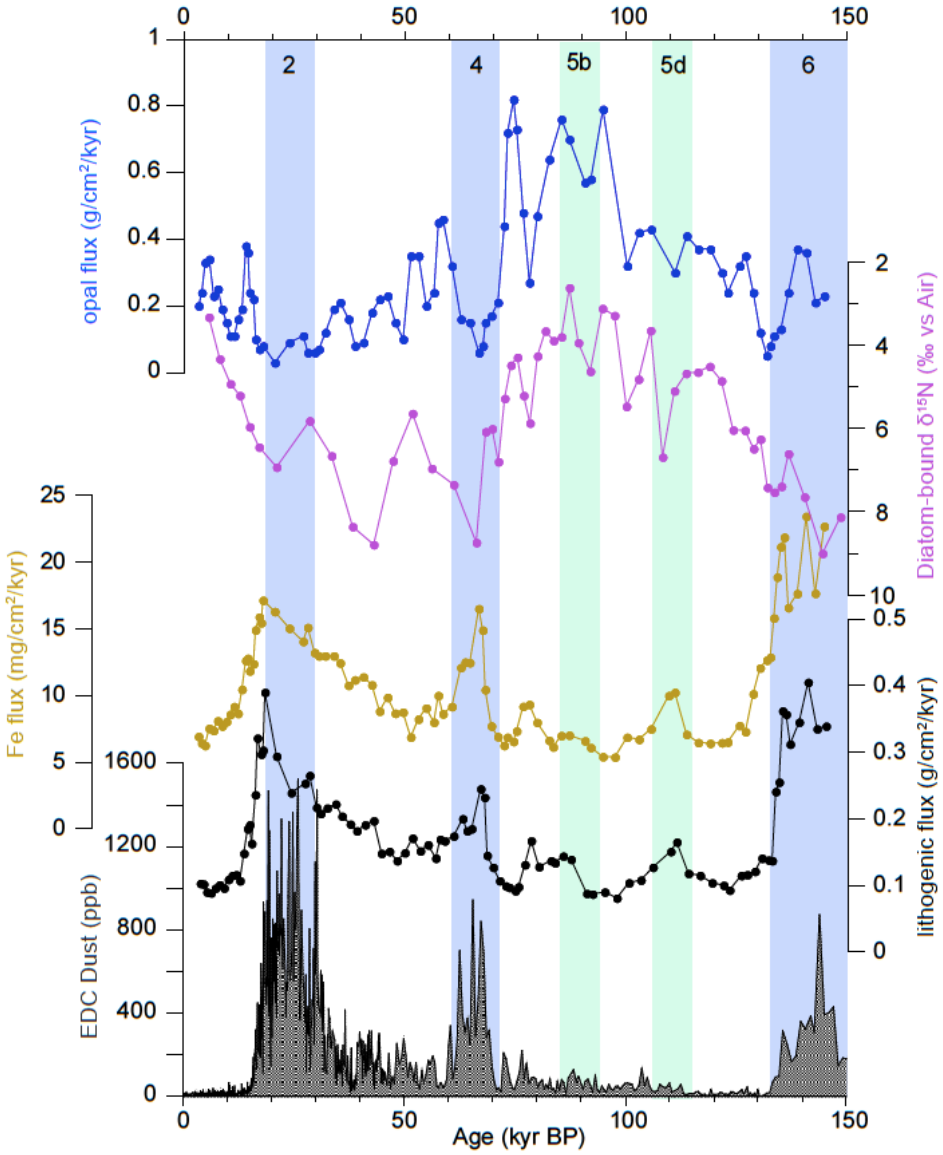

Fig. 12. Comparison of lithogenic fluxes to Antarctica and the SO with nutrient consumption ($\delta^{15}N$) and opal fluxes in core SO136-111. Antarctic dust concentrations recorded in EDC [*Lambert et al.*, 2008] co-varies with the lithogenic and iron (Fe) fluxes from this study. The lithogenic fraction was inferred by assuming a constant detrital ^{232}Th concentration of 10.7 ppm [*Taylor and McLennan*, 1995]. Diatom-bound $\delta^{15}N$ values [*Crosta and Shemesh*, 2002] as an indicator for nutrient consumption (purple line) and opal fluxes (blue line) are shown at the top.

The abovementioned influence of Fe (represented by lithogenic flux), stimulating nutrient consumption but not causing higher BEP becomes evident from the two upper scatter plots in Fig. 13. With an $R^2 = 0.42$, the positive correlation between lithogenic fluxes and $\delta^{15}N$ [*Crosta and Shemesh*, 2002] is stronger than the negative correlation between opal and lithogenic flux ($R^2 = 0.24$), which owing to the pattern is assumed to be exponential. The linear $R^2 = 0.20$ is only marginally lower. This confirms the pattern observed in Fig. 12, where low opal fluxes coincide with maxima in eolian Fe supply. Similarly to $\delta^{15}N$, the diatom-bound nitrogen content [*Crosta et al.*, 2002] increases together with lithogenic fluxes ($R^2 = 0.41$), revealing stronger N uptake/storage. This is consistent to the reported lower Si:N uptake ratio by diatoms under Fe addition [*Brzezinski et al.*, 2002]. By contrasting $\delta^{15}N$ with opal fluxes a strong negative relationship with a high $R^2 = 0.53$ has been found. It is intuitively clear, that a higher nutrient consumption does not reduce opal flux, thus additional

parameters influencing this relationship must be considered. A possibility to increase nutrient consumption while decreasing BEP is by a reduced nutrient supply from below [*Sigman and Boyle*, 2000]. This invokes physical changes such as a modified ocean circulation and different AZ surface conditions during glacial times (further discussed below).

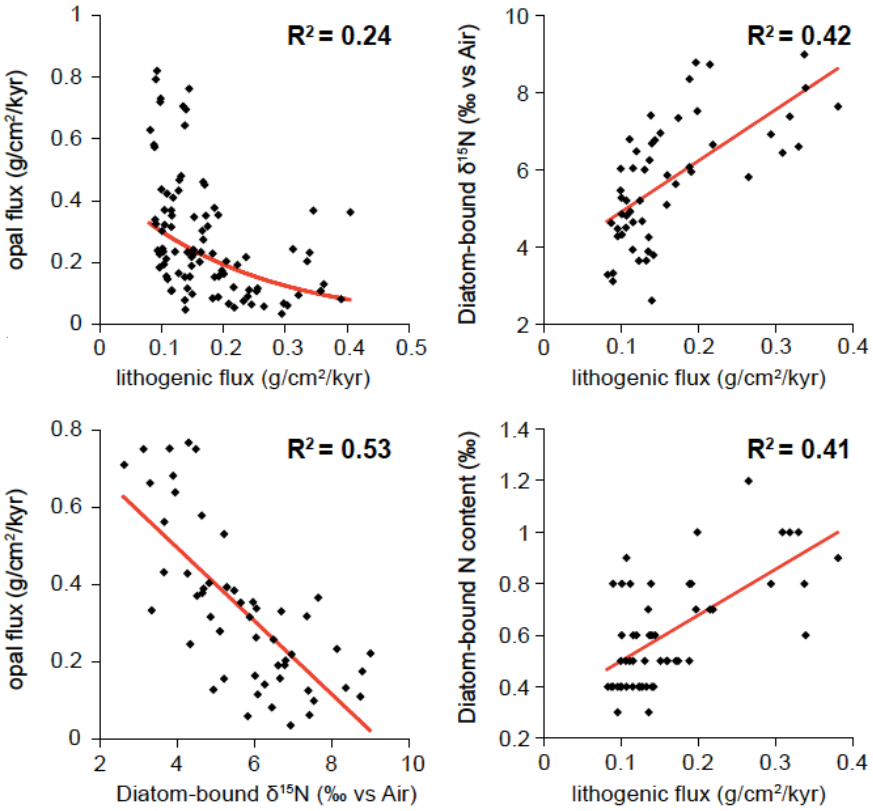

Fig. 13. Scatter plots between lithogenic flux, opal flux, diatom-bound $\delta^{15}N$ and N content. Opal and lithogenic fluxes are from this study, whereas nitrogen isotope data are from [*Crosta and Shemesh*, 2002] and nitrogen content (‰) from [*Crosta et al.*, 2002].

6. Discussion

6.1. Glacial-interglacial changes in biological export production

A strong climate-related signal of BEP and C_{org} export to the ocean interior has been revealed by opal and bioBa fluxes. Opal production is mainly limited by the availability of dissolved silicate and Fe (which is more deficient at present times). Thus, opal export primarily reflects the rate of subsurface nutrient supply within the AZ [*Anderson et al.*, 2009]. Whereas a dramatic change in the glacial ocean nutrient inventory and in turn in the upwelling/mixing waters, has been considered unlikely [*Sigman and Boyle*, 2000], several lines of evidence for a reduced subsurface nutrient supply to the AZ during the cold stages of the last glacial cycle have been presented [e.g., *Francois et al.*, 1997; *Robinson and Sigman*, 2008; *Studer et al.*, 2015]. These studies all inferred a reduction in BEP combined with a more complete nutrient consumption in the AZ. This pattern is supported by the data of SO136-111, which show low BEP and high $\delta^{15}N$ during glacial periods MIS 2-4 and partially MIS 6, indicating a reduced nutrient supply to the SW Pacific APF during these cold intervals. $\delta^{15}N$ was possibly influenced by enhanced eolian Fe flux, yet the reduced nutrient supply is also evident from

opal flux variations alone, if these are assumed to represent nutrient supply from below [*Anderson et al.*, 2009].

The major reduction in BEP in core SO136-111 occurred at the MIS 4/5 transition, consistent with core PS75/072-4 from the central Pacific AZ [*Studer et al.*, 2015]. However, core ODP 1094 [*Jaccard et al.*, 2013] and other cores from the Atlantic AZ showed a substantial decrease in export productivity from MIS 5e onwards [*Frank et al.*, 2000]. Therein, BEP in the Atlantic PFZ was also investigated, which revealed a more comparable pattern to the evolution of bioBa and opal from core SO136-111 during MIS 5. Since ODP 1094 is clearly located in the AZ, whereas both SO136-111 and PS75/072-4 are closer to the modern APF, the reduction in nutrient supply might have occurred earlier in the southern part of the AZ. A gradual northward movement of the APF [*Bostock et al.*, 2013; *Kohfeld et al.*, 2013], accompanied by maximum opal productivity migrating over core site SO136-111, may have left its footprint in high opal fluxes during late MIS 5. Conversely, during warmer climates, the APF and opal belt were shifted southwards [*Frank et al.*, 2000; *Bradtmiller et al.*, 2009], supported by a southward displacement of the STF south of Tasmania during the Holocene and MIS 5 [*Sikes et al.*, 2009]. Although speculative, this could explain the relatively low opal fluxes during MIS 5e (and the Holocene), which is the warmest interval of the last glacial cycle (see Fig. 9), in that the opal belt was at its southernmost position.

Deglacial increases in SW Pacific opal fluxes support the finding of increased Si supply to the AZ for Term I and II, still the rise is significantly lower compared to the Atlantic AZ [*Anderson et al.*, 2009] and central Pacific AZ [*Studer et al.*, 2015]. Similarly, higher BEP together with decreasing $\delta^{15}N$ in core SO136-111 indicate enhanced nutrient supply to the AZ at deglacial transitions, consistent with earlier observations from the AZ [*Francois et al.*, 1997; *Robinson and Sigman*, 2008; *Studer et al.*, 2015]. Distinct peaks of $CaCO_3$ accumulation at the onset of deglaciations were found for both Term I and II (Fig. 8), which is interpreted as a transient deepening of the lysocline, reducing $CaCO_3$ dissolution in the deep ocean [*Jaccard et al.*, 2013]. The sensitivity of $CaCO_3$ accumulation to changes in the lysocline depth is confirmed by the modern lysocline located at about 3600 m in the Emerald Basin close to the core depth of 3912 m [*Sturm*, 2003]. Although production-driven changes in $CaCO_3$ accumulation are possible, the transient signal of the $CaCO_3$ increase, in particular at Term II, speaks for enhanced preservation owing to an increase in deep ocean pH from the release of biologically sequestered CO_2 [*Kohfeld and Ridgwell*, 2009].

Core SO136-111 at the modern APF and therefore at the northernmost part of the AZ seems to reveal characteristic AZ glacial-interglacial changes, although slightly different than in the more southern AZ. These differences are most obvious in the later productivity decrease and a less pronounced deglacial opal increase compared to regions further to the south [*Bradtmiller et al.*, 2009; *Jaccard et al.*, 2013]. This raises the possibility of SAZ-bearing patterns to be recorded in the BEP reconstructions of core SO136-111. Support for this assumption is given by the higher BEP during late MIS 5 relative to the Holocene, which is globally representative for the SAZ rather than the AZ [*Kohfeld et al.*, 2005]. Yet the distinct drop of BEP coinciding with the onset of Fe fertilization at the MIS 4/5 transition, clearly contradicts the common glacial BEP increase in the SAZ [*Anderson et al.*, 2014; *Martínez-García et al.*, 2014]. Furthermore the inferred negative correlation between lithogenic and opal fluxes (see Fig. 13), in contrast is positive in the Pacific SAZ [*Lamy et al.*, 2014], indicating core SO136-

111 to be strongly influenced by AZ productivity changes. To conclude, Fe fertilization in the SW Pacific at the APF might have enhanced nutrient consumption, yet lower nutrient supply dominated the evolution of BEP.

6.2. Glacial changes in Antarctic Zone's nutrient supply

In order to explain the aforementioned decrease in glacial nutrient supply to the surface AZ, a variety of hypotheses have been proposed. Nutrient supply in the AZ depends not only on the vertical upwelling of deep waters [*Anderson et al.*, 2009], but also on wintertime mixing [*Lourey and Trull*, 2001]. With the presented data it is not possible to distinguish between these two mechanisms, yet the fact that opal fluxes, and in turn nutrient supply from below, almost approached zero during the coldest glacial stages, suggests a reduction of both sources. This is also manifested in the sharp $\delta^{15}N$ increase at MIS 4/5. The higher diatom-bound $\delta^{15}N$ suggests either a more complete nutrient consumption or better conditions for nitrate assimilation or both [*Robinson and Sigman*, 2008]. More favorable environments could be the result of reduced Fe limitation, which today is the main limiting factor for SO productivity [*Moore et al.*, 2013]. Likewise surface stratification possibly favored nitrate assimilation by shoaling the surface mixed layer and in turn enhancing light availability for photosynthesis. Both processes seem reasonable for the glacial SW Pacific. Increasing eolian Fe supply has been recorded in core SO136-111 (see Fig. 12), yet there are concerns about the bioavailability of Fe-bearing dust [*Fischer et al.*, 2010], since its dissolved fraction depends also on other factors than the total eolian Fe supply [*Parekh et al.*, 2008]. Support for the Fe induced assimilation enhancement, is provided by recent observations from the Atlantic SAZ, which revealed a distinct correlation between eolian Fe flux and foraminifera-bound $\delta^{15}N$ [*Martínez-García et al.*, 2014] as well as between lithic fluxes and biological productivity [*Anderson et al.*, 2014].

Surface stratification not only favors nitrate assimilation, but also reduces wintertime mixing, thereby lowering nutrient supply [*Robinson and Sigman*, 2008]. The more stratified surface ocean might have arisen from a pronounced halocline in the AZ, related to seasonal sea ice formation and cooling of the polar oceans [*Sigman and Boyle*, 2000; *Sigman et al.*, 2004], both are reasonable conditions for the study site. Further evidence for enhanced glacial stratification in the SW Pacific APF is given by SO136-111 downcore observations of diatom assemblages. An expansion of stratified water-dwelling diatom species during the cold periods MIS 2, 4, and 6 has been reported [*Crosta et al.*, 2004]. Another hypothesis for the reduced deep water nutrient supply to the AZ, involves a reduction and/or northward shift of SH westerlies [*Toggweiler et al.*, 2006; *Anderson et al.*, 2009]. Whereas no consensus about the glacial evolution of the SH westerlies has been reached, a northward shift during colder climate seems likely [*Kohfeld et al.*, 2013]. A glacial weakening of the westerlies would not have reduced upwelling directly, since a concomitant reduction in Ekman transport would have been buffered by reduced eddy fluxes. As a result of countering eddies, residual upwelling and nutrient supply remained unchanged [*Watson and Naveira Garabato*, 2006]. The proposed northward shift would imply reduced northward Ekman transport in the AZ and in turn less upwelling of nutrient-bearing deep waters [*Anderson et al.*, 2009; *Marshall and Speer*, 2012]. Reduction of the westerly wind over the AZ may have strengthened the

halocline through less dissipation of sea ice and fresh surface layer [*Toggweiler et al.*, 2006]. Furthermore, decreased air-sea heat fluxes from colder temperatures and expanded sea ice coverage were suggested to reduce upwelling of deep waters [*Watson and Naveira Garabato*, 2006]. The weakened buoyancy forcing during glacial periods would have decreased residual upwelling, which in turn lowered nutrient supply to the AZ. Yet another hypothesis for the reduced nutrient supply after MIS 4/5 involves cooling NADW at this transition [*Adkins*, 2013]. This may caused saltier southern sourced deep waters through less sea ice melting [*Adkins*, 2013], whereby Antarctic overturning could have declined owing to increased deep ocean stratification that lowered the demand for deep water [*Sigman et al.*, 2010].

The core investigated in this study revealed a remarkably high relationship between opal fluxes (similarly nutrient supply) and Antarctic temperatures during MIS 2 – 4, as well as the cooling into MIS 5 and both deglaciations (see Fig. 9). Since buoyancy in the SO is largely driven by SO temperatures, as they affect air-sea heat exchange and sea ice formation [*Watson and Naveira Garabato*, 2006], the strong coherency between opal flux and Antarctic temperatures can be explained by altered buoyancy fluxes, modifying residual AZ upwelling and nutrient supply. Consequently, cooling at the MIS 4/5 transition lowers both Si and Fe supply from below due to reduced upwelling and mixing in the AZ, recorded in the sharp opal flux reduction and high $\delta^{15}N$. In contrast, during Antarctic warming events [*Jouzel et al.*, 2007], a warmer SO promoted upwelling, wherefore nutrient supply and opal fluxes increased. This reasoning requires Antarctic temperatures to be representative for the SO, which is supported by prior studies [*Martínez-Garcia et al.*, 2009]. A synergy of buoyancy with wind and stratification driven changes of nutrient supply may have evolved during these millennial-scale events, since all were influenced by Antarctic temperatures [*Watson and Naveira Garabato*, 2006; *Robinson and Sigman*, 2008; *Anderson et al.*, 2009]. The occurrence of Antarctic warming events have been linked over the bipolar seesaw to NH freshwater forcing, whereby decreased North Atlantic overturning warmed the SO [*Rahmstorf*, 2002], which according to *Watson and Naveira Garabato* [2006] promoted residual upwelling in the AZ. In addition, modeling studies supported the finding of decreased North Atlantic overturning to provoke reduced SO stratification, by lessening the salt input into the SO [*Schmittner and Galbraith*, 2008]. To summarize, BEP and $\delta^{15}N$ of core SO136-111 confirm the close correlation of AZ nutrient supply, with SO temperatures and Antarctic overturning, whose leverage on pCO_{2atm} is outlined in the next chapter.

6.3. Implications for atmospheric pCO_2

Today, the AZ represents the region with the strongest leak in the global biological pump [*Martínez-Garcia et al.*, 2011]. Hence, closing this atmospheric window to the ocean interior would contribute to lower pCO_{2atm} [*Hain et al.*, 2010]. The glacial reduction in nutrient supply, indicated by lower opal fluxes, as well as generally low BEP concomitant to high $\delta^{15}N$, suggests diminished exchange between the deep ocean and atmosphere carbon reservoirs, since nutrients and DIC transport are closely coupled [*Sigman and Boyle*, 2000]. The evolution of BEP and $\delta^{15}N$ suggests a reduced nutrient supply starting at the MIS 4/5 transition, thus the first pCO_{2atm} drawdown [*Bereiter et al.*, 2015] after MIS 5e can not be attributed to stratification or reduced upwelling in the region of the SW Pacific APF. Rather

reduced overturning in the more southern AZ, inferred by decreasing BEP during early MIS 5, might have provoked the first pCO_{2atm} decrease [*Jaccard et al.*, 2013]. Yet the second pCO_{2atm} decrease at about 70 kyr BP, possibly relates to lower nutrient and DIC supply around the APF, as recorded in SO136-111. The data from *Studer et al.* [2015] confirm the distinct drop in BEP and higher nutrient consumption around MIS 4/5. Likely, the latter pCO_{2atm} decrease is also linked to increased BEP in the SAZ owing to Fe fertilization, which begins at this transition [*Martínez-García et al.*, 2014].

The close relationship between Antarctic temperatures and pCO_{2atm} can be explained if Antarctic overturning is mostly driven by buoyancy forcing [*Fischer et al.*, 2010]. The distinct coherency of opal fluxes from this study to Antarctic temperatures and pCO_{2atm} supports this finding, in that in a warming SO, upwelling of nutrients and DIC was enhanced (indicated by elevated opal fluxes) leading to outgassing of previously deeply sequestered CO_2. Since this relation was previously reported from the Atlantic AZ [*Anderson et al.*, 2009], it is suggested as a common feature of the glacial AZ. A similar mechanism is proposed for the last two deglaciations. Both terminations reveal an increase in BEP owing to stronger Antarctic overturning, which is related to the mechanisms described before. As a consequence of the stronger upward transport of deep ocean waters that were enriched in DIC, outgassing in the AZ was enhanced and pCO_{2atm} rose [*Sigman et al.*, 2010]. The distinct productivity spike during the last deglaciation co-occurred with the onset of HS1, where Antarctic overturning increased and SO stratification broke down for the first time after the LGM, as illustrated by observations of decreased deglacial ventilation ages [*Skinner et al.*, 2010]. This stronger deglacial overturning has also been reported for the SW Pacific [*Rose et al.*, 2010]. Enhanced ventilation likewise affected deep ocean oxygenation, by increasing O_2 transfer to deep waters, manifested amongst others in redox sensitive trace metals [*Jaccard and Galbraith*, 2012; *Galbraith and Jaccard*, 2015]. As outlined above V and aU in core SO136-111 do not directly record past changes in deep water oxygenation, yet, although speculative, the larger Mn excess (Fig. 10) at both deglaciations could indicate enhanced oxygenation of deep waters at the SW Pacific APF, since this region is influenced by mixing with AABW [*Bostock et al.*, 2013].

The presented record confirms previously noted findings of a higher efficiency of the biological pump in the SO during glacial times [e.g., *Francois et al.*, 1997; *Robinson and Sigman*, 2008; *Sigman et al.*, 2010; *Jaccard et al.*, 2013]. Regarding the mechanisms by which the SO biological pump can be strengthened; (i) decreasing overturning (deep ocean ventilation), (ii) more complete nutrient consumption in surface waters [*Sigman et al.*, 2010], the presented dataset, with the inclusion of previous observations provides evidence for a synergy of both processes. Thus the region around SW Pacific APF supports the notion of a higher efficiency of the biological pump in the SO during glacial times, whereby pCO_{2atm} was lowered.

Various other mechanisms possibly influenced pCO_{2atm} over glacial-interglacial cycles, whereof those related to observations of SO136-111 are briefly outlined. First, the expansion of sea ice during glacial periods might have prevented strong CO_2 outgassing, in particular during wintertime when biological productivity declined and sea ice coverage was larger [*Stephens and Keeling*, 2000]. This physical barrier would allow the formation of deep water with high preformed nutrient concentration, yet excess CO_2 would also be transported into the

interior ocean [*Sigman et al.*, 2010]. The SW Pacific shows enhanced glacial sea ice coverage (Fig. 9), still the influence of sea-ice has been questioned, due to the requirement of almost complete coverage in regions of deep water formation [*Morales Maqueda and Rahmstorf*, 2002]. Since sea-ice affects biological productivity, it still might be a considerable parameter in regulating pCO_{2atm}, in particular if seasonal sea ice strengthens the surface halocline [*Robinson and Sigman*, 2008].

Another hypothesis by which SO changes possibly affected pCO_{2atm} is given by the silicic acid leakage hypothesis (SALH) [*Matsumoto et al.*, 2002]. A glacial reduction in AZ opal fluxes has been suggested to leave the surface ocean enriched in silicate. However, this seems to hold true only for the Pacific, since in the Atlantic and Indian Ocean sector of the SO total opal fluxes were not significantly different [*Frank et al.*, 2000; *Chase et al.*, 2003; *Bradtmiller et al.*, 2009]. The excess silicate in the Pacific would have been transported to low latitude surface waters [*Sarmiento et al.*, 2004], where owing to an expanse of diatoms relative to calcifying phytoplankton the C_{org}:$CaCO_3$ ratio in BEP would increase, which in turn could reduce pCO_{2atm} [*Kohfeld and Ridgwell*, 2009]. The reduction in opal flux in the SW Pacific is consistent with the general Pacific pattern, thus gives rise for the SALH, further supported by the lower Si:N uptake ratio [*Crosta et al.*, 2002]. However, an increase in the C_{org}:$CaCO_3$ ratio in low latitude oceans has yet to be found [*Bradtmiller et al.*, 2009]. Similarly, observations from the equatorial Pacific revealed no coherency of increased opal fluxes to pCO_{2atm} [*Kienast et al.*, 2006].

Lastly, it is important to be aware that the aforementioned processes in the SO were only related to the soft-tissue cycle of the biological pump. If the carbonate pump responded similarly, wherefore evidence is presented [*Salter et al.*, 2014], then this would lessen the impact of a more efficient soft tissue pump, also supported by modeling experiments [*Hain et al.*, 2010]. This study, however, still finds a significant pCO_{2atm} drawdown related to changes in the biological pump, even though $CaCO_3$ cycling is considered. In general it is believed that the strengthened soft-tissue pump's leverage on pCO_{2atm} dominated over carbonate pump changes during glacial times [*Hain et al.*, 2014]. In contrast, carbonate compensation feedbacks from variations in BEP and ocean circulation are highly relevant to explain lower glacial pCO_{2atm}, since they essentially co-occur with every change in biological productivity and therefore a crucial factor to explain the magnitude of lower pCO_{2atm} during glacial periods [*Sigman et al.*, 2010].

7. Conclusions

- A close connection between biological export production, global climate and Antarctic temperatures has been inferred over large parts of the last glacial cycle. During colder climate, productivity at the APF was significantly reduced concomitant with lower atmospheric CO_2 concentrations. In particular, the MIS 4/5 transition at 71 kyr BP and the subsequent transient Antarctic warming events of MIS 3 reveal a strong correlation between pCO_{2atm} and export fluxes of opal and bioBa.
- The reduction in surface productivity accompanied by higher nutrient consumption is interpreted to be a consequence of reduced nutrient supply from below, related to enhanced surface stratification and diminished Antarctic overturning. Likewise,

stronger eolian dust (and Fe) supply has been inferred to occur during coldest periods, which possibly stimulated nutrient consumption but not increasing BEP, since subsurface reduction in nutrient supply was a more crucial factor. The weakened overturning and more complete nutrient consumption lowered outgassing of CO_2, thus the modern leak of the biological pump in the AZ was reduced during glacial times. Potential reasons for this change in glacial ocean circulation were modified buoyancy or stratification (halocline) conditions, as well as changes in westerly winds, which are all coupled to Antarctic temperatures.

- Consistent with previous observations from the AZ, a distinct increase in productivity co-occurred with lower nutrient consumption at glacial terminations. This indicates stronger nutrient supply from below and a greater leak in the biological pump, leading pCO_{2atm} to rise. Additionally, deglaciations recorded a transient $CaCO_3$ accumulation peak, possibly related to a loss of CO_2 from the deep ocean.
- Redox-sensitive trace metals did not reveal past deviations from modern oxic conditions, yet they support the use of bioBa as a proxy for organic matter export. Rather than changes in oxygenation, aU tracks the remineralization of C_{org} within the sediment.

7.1. Outlook

The investigation of sedimentary constituents in core SO136-111 confirmed the high sensitivity of biological productivity to glacial-interglacial changes in the SO. The study contributed to the expansion of the spatial and temporal coverage of paleoceanographic records, by reconstructing some well-known features from other regions of the glacial SO. A central outcome is the importance of the study site relative to modern oceanographic settings, in particular the APF. Therefore in future investigations it would be interesting to see how cores from the SW Pacific, located clearly north and south of the APF have responded to different climate conditions. Likewise, conducted measurements should be expanded further back to cover the whole MIS 6, since there seem to be dissimilarities compared to the LGM. In addition, a high-resolution proxy for nutrient consumption in the SW Pacific would provide insights into millennial-scale changes in nutrient conditions. If possible, foraminifera bound $\delta^{15}N$ from the planktonic N. pachyderma would deliver supplementary information to the lower resolved diatom bound $\delta^{15}N$ and possibly confirm inferences from this proxy. Finally, a more robust age model is under development, whereby more certain conclusions of distinct transitions and deglacial sequences can be drawn. The presented age model bears some uncertainties through the assumption of planktonic $\delta^{18}O$ closely following Antarctic temperatures. Recently received data for magnetic susceptibility and possibly strontium/rubidium ratio should allow to refine the existing age model, yet the general outcomes of this study should not be affected significantly.

In the context of current climate change, the investigations revealed a high sensitivity of the Southern Ocean to changing temperatures in the past. Accordingly, the pronounced polar warming of the next centuries [*IPCC*, 2013] will include significant feedback mechanisms from a responding biology and ocean circulation, likely influencing future atmospheric pCO_2.

8. Acknowledgements

I would like to thank the whole “Paleoceanography and marine biogeochemistry” research group for all the help and advice they have offered me, with special thank you to my main supervisor Samuel L. Jaccard and co-supervisor Jörg Lippold. Likewise I am grateful for the support of everyone else, who made this Master Thesis possible. At this occasion, I also appreciate the opportunity to conduct my master program at the Oeschger Centre and the Institute of Geological Sciences, University of Bern.

9. Bibliography

Adkins, J. F. (2013), The role of deep ocean circulation in setting glacial climates, *Paleoceanography*, *28*(3), 539–561, doi:10.1002/palo.20046.

Altabet, M. A., and F. Francois (1994), Sedimentary nitrogen isotopic ratio as a recorder for surface ocean ntirate utilization., *Biogeochem. Cycles.*, *8*(1), 103–116.

Anderson, R. F., S. Ali, L. I. Bradtmiller, S. H. H. Nielsen, M. Q. Fleisher, B. E. Anderson, and L. H. Burckle (2009), Wind-driven upwelling in the Southern Ocean and the deglacial rise in Atmospheric CO2, *Science*, *323*, 1443 – 1448.

Anderson, R. F., S. Barker, M. Fleisher, R. Gersonde, S. L. Goldstein, G. Kuhn, P. G. Mortyn, K. Pahnke, and J. P. Sachs (2014), Biological response to millennial variability of dust and nutrient supply in the Subantarctic South Atlantic Ocean., *Philos. Trans. R. Soc. Ser. A,*, *372*, 20130054, doi:10.1098/rsta.2013.0054.

Bacon, M. P. (1984), Glacial to interglacial changes in carbonate and clay sedimentation in the Atlantic Ocean estimated from 230Th measurements, *Chem. Geol.*, *46*(2), 97–111, doi:http://dx.doi.org/10.1016/0009-2541(84)90183-9.

Bereiter, B., S. Eggleston, J. Schmitt, C. Nehrbass-ahles, T. F. Stocker, H. Fischer, S. Kipfstuhl, and J. Chappellaz (2015), Revision of the EPICA Dome C CO2 record from 800 to 600 kyr before present, *Geophys. Res. Lett.*, *42*, 542–549, doi:10.1002/2014GL061957.

Berger, A. (1988), Milankovitch theory and climate, *Rev. Geophys.*, *26*(4), 624–657.

Bernsdorff, F. (2008), Dissertation: Rekonstruktion der Erdmagnetfeldstärke der vergangenen 300.000 Jahre über den kosmogenen Tracer 10Be aus Atlantischen Tiefseesedimenten (ODP-Sites 983 und 1063).

Böhm, E., J. Lippold, M. Gutjahr, M. Frank, P. Blaser, B. Antz, J. Fohlmeister, N. Frank, M. B. Andersen, and M. Deininger (2015), Strong and deep Atlantic meridional overturning circulation during the last glacial cycle, *Nature*, *517*(7532), 73–76, doi:10.1038/nature14059.

Bostock, H. C. et al. (2013), A review of the Australian-New Zealand sector of the Southern Ocean over the last 30ka (Aus-INTIMATE project), *Quat. Sci. Rev.*, *74*, 35–57, doi:10.1016/j.quascirev.2012.07.018.

Bourne, M. D., A. L. Thomas, C. Mac Niocaill, and G. M. Henderson (2012), Improved determination of marine sedimentation rates using 230Th xs, *Geochemistry, Geophys. Geosystems*, *13*(1), Q09017, doi:10.1029/2012GC004295.

Bradtmiller, L. I., R. F. Anderson, M. Q. Fleisher, and L. H. Burckle (2009), Comparing glacial and Holocene opal fluxes in the Pacific sector of the Southern Ocean, *Paleoceanography*, *24*, PA2214, doi:10.1029/2008PA001693.

Bradtmiller, L. I., R. F. Anderson, J. P. Sachs, and M. Q. Fleisher (2010), A deeper respired carbon pool in the glacial equatorial Pacific Ocean, *Earth Planet. Sci. Lett.*, *299*(3-4), 417–425, doi:10.1016/j.epsl.2010.09.022.

Broecker, W. S. (1991), The great ocean conveyor, *Oceanography*, *4*(2), 79–89.

Broecker, W. S., and G. H. Denton (1990), What Drives Glacial Cycles?, *Sci. Am.*, *262*(1), 48–56, doi:10.1038/scientificamerican0190-48.

Brzezinski, M. A., C. J. Pride, V. M. Franck, D. M. Sigman, N. Gruber, G. H. Rau, and K. H. Coale (2002), A switch from Si(OH)4 to NO3 depletion in the glacial Southern Ocean, *Geophys. Res. Lett.*, *29*(12), 3–6.

Carlson, C. A., N. R. Bates, D. A. Hansell, and D. K. Steinberg (2001), Carbon Cycle, in *Encyclopedia of Ocean Sciences*, pp. 390–400, Academic Press.

Chase, Z., R. F. Anderson, and M. Q. Fleisher (2001), Evidence from authigenic uranium for increased productivity of the glacial Subantarctic Ocean, *Paleoceanography*, *16*(5), 468–478, doi:10.1029/2000PA000542.

Chase, Z., R. F. Anderson, M. Q. Fleisher, and P. W. Kubik (2003), Accumulation of biogenic and lithogenic material in the Pacific sector of the Southern Ocean during the past 40,000 years, *Deep. Res. Part II Top. Stud. Oceanogr.*, *50*(3-4), 799–832, doi:10.1016/S0967-0645(02)00595-7.

Clark, P. U. (1999), Northern Hemisphere Ice-Sheet Influences on Global Climate Change, *Science*, *286*(5442), 1104–1111, doi:10.1126/science.286.5442.1104.

Clark, P. U., and A. C. Mix (2002), Ice sheets and sea level of the Last Glacial Maximum., *Quat. Sci. Rev.*, *21*, 1–7, doi:10.1016/S0277-3791(01)00118-4.

Clark, P. U., A. S. Dyke, J. D. Shakun, A. E. Carlson, J. Clark, B. Wohlfarth, J. X. Mitrovica, S. W. Hostetler, and a M. McCabe (2009), The Last Glacial Maximum., *Science*, *325*(5941), 710–4, doi:10.1126/science.1172873.

Crosta, X., and A. Shemesh (2002), Reconciling down core anticorrelation of diatom carbon and nitrogen isotopic ratios from the Southern Ocean, *Paleoceanography*, *17*(1), 1010, doi:10.1029/2000PA000565.

Crosta, X., A. Shemesh, M.-E. Salvignac, H. Gildor, and R. Yam (2002), Late quaternary variations of elemental ratios (C/Si and N/Si) in diatom-bound organic matter from the Southern Ocean, *Deep Sea Res. Part II Top. Stud. Oceanogr.*, *49*(9-10), 1939–1952, doi:10.1016/S0967-0645(02)00019-X.

Crosta, X., A. Sturm, L. Armand, and J.-J. Pichon (2004), Late Quaternary sea ice history in the Indian sector of the Southern Ocean as recorded by diatom assemblages, *Mar. Micropaleontol.*, *50*(3-4), 209–223, doi:10.1016/S0377-8398(03)00072-0.

Curry, W. B., and D. W. Oppo (2005), Glacial water mass geometry and the distribution of δ13C of CO2 in the western Atlantic Ocean, *Paleoceanography*, *20*(1), PA1017, doi:10.1029/2004PA001021.

Dlugokencky, E., and P. Tans (2015), NOAA/ESRL, Available from: www.esrl.noaa.gov/gmd/ccgg/trends/ (Accessed 7 June 2015)

Dymond, J., E. Suess, and M. Lyle (1992), Barium in deep-sea sediment: a geochemical proxy for paleoproductivity, *Paleoceanography*, *7*(2), 163–181.

Fairbanks, R. G. (1989), A 17,000-year glacio-eustatic sea level record: influence of glacial melting rates on the Younger Dryas event and deep-ocean circulation., *Nature*, *342*, 637–642.

Fischer, H. et al. (2010), The role of Southern Ocean processes in orbital and millennial CO2 variations - A synthesis, *Quat. Sci. Rev.*, *29*(1-2), 193–205, doi:10.1016/j.quascirev.2009.06.007.

Francois, R., M. P. Bacon, M. A. Altabet, and L. D. Labeyrie (1993), Glacial/Interglacial changes in sediment rain rate in the SW Indian sector of Subantarctic waters as recorded by 230Th, 231Pa, U, and δ15N, *Paleoceanography*, *8*(5), 611–629.

Francois, R., S. Honjo, S. J. Manganini, and G. E. Ravizza (1995), Biogenic barium fluxes to the deep sea: Implications for paleoproductivity reconstruction, *Global Biogeochem. Cycles*, *9*(2), 289–303.

Francois, R. et al. (1997), Contribution of Southern Ocean surface-water stratification to low atmospheric CO2 concentrations during the last glacial period, *Nature*, *389*(6654), 929–935, doi:10.1038/40073.

Francois, R., M. Frank, M. M. Rutgers van der Loeff, and M. P. Bacon (2004), 230Th normalization: An essential tool for interpreting sedimentary fluxes during the late Quaternary, *Paleoceanography*, *19*(1), PA1018, doi:10.1029/2003PA000939.

Frank, M., R. Gersonde, M. M. Rutgers van der Loeff, G. Bohrmann, C. C. Nürnberg, P. W. Kubik, M. Suter, and A. Mangini (2000), Similar glacial and interglacial export bioproductivity in the Atlantic sector of the Southern Ocean : Multiproxy evidence and implications for glacial atmospheric CO2, *Paleoceanography*, *15*(6), 642–658.

Galbraith, E. D., and S. L. Jaccard (2015), Deglacial weakening of the oceanic soft tissue pump: global constraints from sedimentary nitrogen isotopes and oxygenation proxies, *Quat. Sci. Rev.*, *109*, 38–48, doi:10.1016/j.quascirev.2014.11.012.

Ganeshram, R. S., R. François, J. Commeau, and S. L. Brown-Leger (2003), An experimental investigation of barite formation in seawater, *Geochim. Cosmochim. Acta*, *67*(14), 2599–2605, doi:10.1016/S0016-7037(03)00164-9.

Hain, M. P., D. M. Sigman, and G. H. Haug (2010), Carbon dioxide effects of Antarctic stratification, North Atlantic Intermediate Water formation, and subantarctic nutrient drawdown during the last ice age: Diagnosis and synthesis in a geochemical box model, *Global Biogeochem. Cycles*, *24*, GB4023, doi:10.1029/2010GB003790.

Hain, M. P., D. M. Sigman, and G. H. Haug (2014), The Biological Pump in the past, in *Treatise on Geochemistry*, vol. 8, pp. 485–517, Elsevier.

Hays, J. D., J. Imbrie, and N. J. J. . Shackleton (1976), Variations in the Earth's Orbit : Pacemaker of the Ice Ages, *Science*, *194*(4270), 1121–1132, doi:10.1126/science.194.4270.1121.

Henderson, G. M., and R. F. Anderson (2003), The U-series Toolbox for Paleoceanography, *Rev. Mineral. Geochemistry*, *52*(1), 493–531, doi:10.2113/0520493.

Holmen, K. (1992), The Global Carbon Cycle, *Int. Geophys. Ser. Glob. Biogeochem. cycles*, *50*, 239–262.

Hoogakker, B. A. A., H. Elderfield, G. Schmiedl, I. N. McCave, and R. E. M. Rickaby (2015), Glacial–interglacial changes in bottom-water oxygen content on the Portuguese margin, *Nat. Geosci.*, *8*, 2–5, doi:10.1038/ngeo2317.

Imbrie, J. et al. (1993), On the structure and origin of major glaciation cycles 2. The 100,000-year cycle, *Paleoceanography*, *8*(6), 699, doi:10.1029/93PA02751.

IPCC (2013), *Climate Change 2013: The Physical Science Basis. Contribution of Working Group I to the Fifth Assessment Report of the Intergovernmental Panel on Climate Change [Stocker, T.F., D. Qin, G.-K. Plattner, M. Tignor, S.K. Allen, J. Boschung, A. Nauels, Y. Xia,* Cambridge, United Kingdom and New York, NY, USA.

Jaccard, S. L., and E. D. Galbraith (2012), Large climate-driven changes of oceanic oxygen concentrations during the last deglaciation, *Nat. Geosci.*, *5*(2), 151–156, doi:10.1038/ngeo1352.

Jaccard, S. L., E. D. Galbraith, D. M. Sigman, G. H. Haug, R. Francois, T. F. Pedersen, P. Dulski, and H. R. Thierstein (2009), Subarctic Pacific evidence for a glacial deepening of the oceanic respired carbon pool, *Earth Planet. Sci. Lett.*, *277*(1-2), 156–165, doi:10.1016/j.epsl.2008.10.017.

Jaccard, S. L., C. T. Hayes, D. A. Hodell, R. F. Anderson, D. M. Sigman, and G. H. Haug (2013), Two modes of change in SO Productivity, *Science*, *339*(6126), 1419–1423.

Jouzel, J. et al. (2007), Orbital and millennial Antarctic climate variability over the past 800,000 years., *Science*, *317*(5839), 793–796, doi:10.1126/science.1141038.

Kienast, S. S., M. Kienast, S. Jaccard, S. E. Calvert, and R. François (2006), Testing the silica leakage hypothesis with sedimentary opal records from the eastern equatorial Pacific over the last 150 kyrs, *Geophys. Res. Lett.*, *33*(15), 2–5, doi:10.1029/2006GL026651.

Knox, F., and M. McElroy (1984), Changes in atmospheric CO2: Influence of the marine biota at high latitude, *J. Geophys. Res.*, *89*(D3), 4629–4637, doi:10.1029/JD089iD03p04629.

Kohfeld, K. E., and A. Ridgwell (2009), Glacial-Interglacial Variability in Atmospheric CO2, in *Surface ocean- lower atmosphere processes*, edited by C. Le Quéré, pp. 251–286, AGU.

Kohfeld, K. E., C. Le Quéré, S. P. Harrison, and R. F. Anderson (2005), Role of marine biology in glacial-interglacial CO2 cycles., *Science*, *308*(5718), 74–8, doi:10.1126/science.1105375.

Kohfeld, K. E., R. M. Graham, A. M. de Boer, L. C. Sime, E. W. Wolff, C. Le Quéré, and L. Bopp (2013), Southern Hemisphere westerly wind changes during the Last Glacial Maximum: paleo-data synthesis, *Quat. Sci. Rev.*, *68*, 76–95, doi:10.1016/j.quascirev.2013.01.017.

Kuhlbrodt, T., A. Griesel, M. Montoya, A. Levermann, M. Hofmann, and S. Rahmstorf (2007), On the driving processes of the Atlantic meridional overturning circulation, *Rev. Geophys.*, *45*, RG2001, doi:10.1029/2004RG000166.

Kumar, N., R. F. Anderson, R. A. Mortlock, P. N. Froelich, P. Kubik, B. Dittrich-Hannen, and M. Suter (1995), Increased biological productivity and export production in the glacial Southern Ocean, *Nature*, *378*(6558), 675–680, doi:10.1038/378675a0.

Lambert, F., B. Delmonte, J. R. Petit, M. Bigler, P. R. Kaufmann, M. A. Hutterli, T. F. Stocker, U. Ruth, J. P. Steffensen, and V. Maggi (2008), Dust-climate couplings over the past 800,000 years from the EPICA Dome C ice core., *Nature*, *452*(7187), 616–619, doi:10.1038/nature06763.

Lamy, F., R. Gersonde, G. Winckler, O. Esper, A. Jaeschke, G. Kuhn, J. Ullermann, A. Martinez-Garcia, F. Lambert, and R. Kilian (2014), Increased dust deposition in the Pacific Southern Ocean during glacial periods., *Science*, *343*(6169), 403–7, doi:10.1126/science.1245424.

Lippold, J., Y. Luo, R. Francois, S. E. Allen, J. Gherardi, S. Pichat, B. Hickey, and H. Schulz (2012), Strength and geometry of the glacial Atlantic Meridional Overturning Circulation, *Nat. Geosci.*, *5*(11), 813–816, doi:10.1038/ngeo1608.

Lisiecki, L. E., and M. E. Raymo (2005), A Pliocene-Pleistocene stack of 57 globally distributed benthic δ18O records, *Paleoceanography*, *20*(PA1003), doi:10.1029/2004PA001071.

Lourey, M. J., and T. W. Trull (2001), Seasonal nutrient depletion and carbon export in the Subantarctic and Polar Frontal zones of the Southern Ocean south of Australia, *J. Geophys. Res.*, *106*(C12), 31463–31487.

Lumpkin, R., and K. Speer (2007), Global Ocean Meridional Overturning, *J. Phys. Oceanogr.*, *37*(10), 2550–2562, doi:10.1175/JPO3130.1.

Lüthi, D. et al. (2008), High-resolution carbon dioxide concentration record 650,000-800,000 years before present., *Nature*, *453*(7193), 379–382, doi:10.1038/nature06949.

Lynch-Stieglitz, J. et al. (2007), Atlantic meridional overturning circulation during the Last Glacial Maximum, *Science*, *316*(5821), 66–70, doi:10.1126/science.1137127.

Marshall, J., and K. Speer (2012), Closure of the meridional overturning circulation through Southern Ocean upwelling, *Nat. Geosci.*, *5*(3), 171–180, doi:10.1038/ngeo1391.

Martin, J. H. (1990), Glacial-Interglacial CO2 Change: The Iron Hypothesis, *Paleoceanography*, *5*(1), 1–13, doi:10.1029/PA005i001p00001.

Martínez-Garcia, A., A. Rosell-Melé, W. Geibert, R. Gersonde, P. Masqué, V. Gaspari, and C. Barbante (2009), Links between iron supply, marine productivity, sea surface temperature, and CO2 over the last 1.1 Ma, *Paleoceanography*, *24*(PA1207), doi:10.1029/2008PA001657.

Martínez-Garcia, A., A. Rosell-Melé, S. L. Jaccard, W. Geibert, D. M. Sigman, and G. H. Haug (2011), Southern Ocean dust-climate coupling over the past four million years., *Nature*, *476*(7360), 312–5, doi:10.1038/nature10310.

Martínez-García, A., D. M. Sigman, H. Ren, R. F. Anderson, M. Straub, D. a Hodell, S. L. Jaccard, T. I. Eglinton, and G. H. Haug (2014), Iron fertilization of the Subantarctic ocean during the last ice age., *Science*, *343*(6177), 1347–50, doi:10.1126/science.1246848.

Matsumoto, K., J. L. Sarmiento, and M. A. Brzezinski (2002), Silicic acid leakage from the Southern Ocean : A possible explanation for glacial atmospheric pCO2, *Global Biogeochem. Cycles*, *16*(3), 1031, doi:10.1029/2001GB001442.

Meyer-Jacob, C., H. Vogel, F. Boxberg, P. Rosén, M. E. Weber, and R. Bindler (2014), Independent measurement of biogenic silica in sediments by FTIR spectroscopy and PLS regression, *J. Paleolimnol.*, *52*, 245–255, doi:10.1007/s10933-014-9791-5.

Monnin, E., A. Indermühle, A. Dällenbach, J. Flückiger, B. Stauffer, T. F. Stocker, D. Raynaud, and J. M. Barnola (2001), Atmospheric CO2 concentrations over the last glacial termination., *Science*, *291*(5501), 112–114, doi:10.1126/science.291.5501.112.

Moore, C. M. et al. (2013), Processes and patterns of oceanic nutrient limitation, *Nat. Publ. Gr.*, *6*(9), 701–710, doi:10.1038/ngeo1765.

Morales Maqueda, M. A., and S. Rahmstorf (2002), Did Antarctic sea-ice expansion cause glacial CO2 decline?, *Geophys. Res. Lett.*, *29*(1), 111–113, doi:10.1029/2001gl013240.

Mortlock, R. A., C. D. Charles, P. N. Froelich, M. A. Zibello, J. Saltzman, J. D. Hays, and L. H. Burckle (1991), Evidence for lower productivity in the Antarctic Ocean during the last glaciation, *Nature*, *351*(6323), 220–223.

Neftel, A., H. Oeschger, J. Schwander, B. Stauffer, and R. Zumbrunn (1982), Ice core sample measurements give atmospheric CO2 content during the past 40,000 yr, *Nature*, *295*, 220–223.

Orsi, A. H., T. Whitworth, and W. D. Nowlin (1995), On the meridional extent and fronts of the Antarctic Circumpolar Current, *Deep Sea Res. Part I Oceanogr. Res. Pap.*, *42*(5), 641–673, doi:10.1016/0967-0637(95)00021-W.

Paillard, D., L. Labeyrie, and P. Yiou (1996), Macintosh Program performs time-series analysis, *Eos, Trans. Am. Geophys. Union*, *77*(39), 379, doi:10.1029/96EO00259.

Parekh, P., F. Joos, and S. A. Müller (2008), A modeling assessment of the interplay between aeolian iron fluxes and iron-binding ligands in controlling carbon dioxide fluctuations during Antarctic warm events, *Paleoceanography*, *23*, PA4202, doi:10.1029/2007PA001531.

Petit, R. J., D. Raynaud, I. Basile, J. Chappellaz, C. Ritz, M. Delmotte, M. Legrand, C. Lorius, and L. Pe (1999), Climate and atmospheric history of the past 420,000 years from the Vostok ice core, Antarctica, *Nature*, *399*, 429–413, doi:10.1038/20859.

Pollard, R. T. et al. (2009), Southern Ocean deep-water carbon export enhanced by natural iron fertilization., *Nature*, *457*(7229), 577–580, doi:10.1038/nature07716.

Rahmstorf, S. (2002), Ocean circulation and climate during the past 120,000 years., *Nature*, *419*(6903), 207–214, doi:10.1038/nature01090.

Raymo, M. E., and P. Huybers (2008), Unlocking the mysteries of the ice ages., *Nature*, *451*(7176), 284–5, doi:10.1038/nature06589.

Robinson, R. S., and D. M. Sigman (2008), Nitrogen isotopic evidence for a poleward decrease in surface nitrate within the ice age Antarctic, *Quat. Sci. Rev.*, *27*(9-10), 1076–1090, doi:10.1016/j.quascirev.2008.02.005.

Robinson, R. S., D. M. Sigman, P. J. DiFiore, M. M. Rohde, T. A. Mashiotta, and D. W. Lea (2005), Diatom-bound 15N/14N: New support for enhanced nutrient consumption in the ice age subantarctic, *Paleoceanography*, *20*(3), 1–14, doi:10.1029/2004PA001114.

Rose, K. A., E. L. Sikes, T. P. Guilderson, P. Shane, T. M. Hill, R. Zahn, and H. J. Spero (2010), Upper-ocean-to-atmosphere radiocarbon offsets imply fast deglacial carbon dioxide release., *Nature*, *466*(7310), 1093–1097, doi:10.1038/nature09288.

Rosen, P., H. Vogel, L. Cunningham, A. Hahn, S. Hausmann, R. Pienitz, B. Zolitschka, B. Wagner, and P. Persson (2011), Universally Applicable Model for the Quantitative Determination of Lake Sediment Composition Using Fourier Transform Infrared Spectroscopy, *Environ. Sci. Technol.*, *45*, 8858–8865.

Salter, I., R. Schiebel, P. Ziveri, A. Movellan, R. Lampitt, and G. A. Wolff (2014), Carbonate counter pump stimulated by natural iron fertilization in the Polar Frontal Zone, *Nat. Geosci.*, *7*, 885–889, doi:10.1038/ngeo2285.

Sarmiento, J. L., and N. Gruber (2006), *Ocean Biogeochemical Dynamics*, Princeton University Press, Princeton and Oxford.

Sarmiento, J. L., and J. R. Toggweiler (1984), A new model for the role of the oceans in determining atmospheric pCO2, *Nature*, *308*(5960), 621–624, doi:10.1038/308621a0.

Sarmiento, J. L., N. Gruber, M. A. Brzezinski, and J. P. Dunne (2004), High-latitude controls of thermocline nutrients and low latitude biological productivity., *Nature*, *427*(6969), 56–60, doi:10.1038/nature10605.

Schlitzer, R. (2000), Electronic Atlas of WOCE Hydrographic and Tracer Data Now Available, *Eos Trans. AGU*, *81(5), 45*.

Schmittner, A., and E. D. Galbraith (2008), Glacial greenhouse-gas fluctuations controlled by ocean circulation changes, *Nature*, *456*, 373–376, doi:10.1038/nature07531.

Shackleton, N. J. (2000), The 100,000-Year Ice-Age Cycle Identified and Found to Lag Temperature, Carbon Dioxide, and Orbital Eccentricity, *Science*, *289*(5486), 1897–1902, doi:10.1126/science.289.5486.1897.

Shakun, J. D., P. U. Clark, F. He, S. a Marcott, A. C. Mix, Z. Liu, B. Otto-Bliesner, A. Schmittner, and E. Bard (2012), Global warming preceded by increasing carbon dioxide concentrations during the last deglaciation., *Nature*, *484*(7392), 49–54, doi:10.1038/nature10915.

Siegenthaler, U., and T. Wenk (1984), Rapid atmospheric CO2 variations and ocean circulation, *Nature*, *308*, 624–626.

Siegenthaler, U. et al. (2005), Stable Carbon Cycle – Climate Relationship During the Late Pleistocene, *Science*, *310*, 1313–1317, doi:10.1126/science.1120130.

Sigman, D. M., and E. A. Boyle (2000), Glacial/IG variations in atmospheric carbon dioxide, *Nature*, *407*, 859–869.

Sigman, D. M., S. L. Jaccard, and G. H. Haug (2004), Polar ocean stratification in a cold climate, *Nature*, 59–63, doi:10.1038/nature02378.1.

Sigman, D. M., M. P. Hain, and G. H. Haug (2010), The polar ocean and glacial cycles in atmospheric CO2 concentration, *Nature*, *466*(7302), 47–55, doi:10.1038/nature09149.

Sikes, E. L., W. R. Howard, C. R. Samson, T. S. Mahan, L. G. Robertson, and J. K. Volkman (2009), Southern ocean seasonal temperature and subtropical front movement on the south tasman rise in the late quaternary, *Paleoceanography*, *24*, PA2201, doi:10.1029/2008PA001659.

Skinner, L. C., S. Fallon, C. Waelbroeck, E. Michel, and S. Barker (2010), Ventilation of the Deep Southern Ocean and deglacial CO2 rise, *Science*, *328*, 1147–1151.

Stephens, B. B., and R. F. Keeling (2000), The influence of Antarctic sea ice on glacial-interglacial CO2 variations, *Nature*, *404*, 171–174, doi:10.1038/35004556.

Studer, A. S., D. M. Sigman, A. Martínez-garcía, V. Benz, G. Winckler, R. Gersonde, and G. H. Haug (2015), Antarctic Zone nutrient conditions during the last two glacial cycles, *Paleoceanography*, *30*(7), 845–862, doi:10.1002/2014PA002745.

Sturm, A. (2003), Dissertation: Changes in ocean circulation and carbonate chemistry in the Australian sector of the Southern Ocean during the last 500,000 years.

Talley, L. D. (2013), Closure of the global overturning circulation through the Indian, Pacific and Southern Oceans: schematics and transports, *Oceanography*, *26*(1), 80–97, doi:10.5670/oceanog.2011.65.

Taylor, S. R., and S. M. McLennan (1985), *The Continental Crust: Its Composition and Evolution: An Examination of the Geochemical Record Preserved in Sedimentary Rocks.*, Blackwell Scientific Editor, Oxford.

Taylor, S. R., and S. M. McLennan (1995), The geochemical evolution of the continental crust, *Rev. Geophys.*, *33*(2), 241–265, doi:10.1029/95RG00262.

Thiede, J. et al. (1999), *FS Sonne Fahrtbericht SO136 / Cruise report SO136 TASQWA : Quaternary variability of water masses in the southern Tasman Sea and the Southern Ocean (SW Pacific Section)*, GEOMAR Forschungszentrum für marine Geowissenschaften der Christian-Albrechts-Universität, Kiel.

Toggweiler, J. R., J. L. Russell, and S. R. Carson (2006), Midlatitude westerlies, atmospheric CO2, and climate change during the ice ages, *Paleoceanography*, *21*, PA2005, doi:10.1029/2005PA001154.

Tribovillard, N., T. J. Algeo, T. Lyons, and A. Riboulleau (2006), Trace metals as paleoredox and paleoproductivity proxies: An update, *Chem. Geol.*, *232*(1-2), 12–32, doi:10.1016/j.chemgeo.2006.02.012.

Vogel, H., J. Lippold, S. L. Jaccard, and L. Thöle (n.d.), Determining biogenic silica by means of FTIR spectroscopy in marine sediments- a validation study, *in prep.*

Watson, A. J., and A. C. Naveira Garabato (2006), The role of Southern Ocean mixing and upwelling in glacial-interglacial atmospheric CO2 change, *Tellus, Ser. B Chem. Phys. Meteorol.*, *58*(1), 73–87, doi:10.1111/j.1600-0889.2005.00167.x.

Zeebe, R. E. (2012), History of Seawater Carbonate Chemistry, Atmospheric CO2 , and Ocean Acidification, *Annu. Rev. Earth Planet. Sci.*, *40*(1), 141–165, doi:10.1146/annurev-earth-042711-105521.

10. Appendix

A) Age tie points and sedimentation rate

Tab. A.1 shows the exact tie points from the age model used in this study. Tie points marked with an asterisk indicate radiocarbon dates from the previously published age model [*Crosta et al.*, 2004]. Since the age calibration assumed a constant reservoir age of 800 years, one additional radiocarbon date at the last deglaciation was disregarded, because the reorganization of ocean circulation likely provoked distinct changes in the reservoir age. In Fig. A.1 sedimentation rate of core SO136-111 is shown. The highest sedimentation rates are concomitant to deglaciations and late MIS 5 with up to 7 cm/kyr, where the highest opal fluxes have been inferred. In contrast, the lowest sedimentation rate can be seen during coldest intervals MIS 2, 4 and 6, which is related to relatively low BEP.

Depth (cm)	Age tie points (kyr BP)
1	3.2*
28	9.9*
67	18.3
78	27.2
111	43.1*
142	56.7
162	66.9
243	78.4
298	88.4
368	107.6
443	127.6
501	136.7
537	151.2

Tab. A.1: Age tie points.

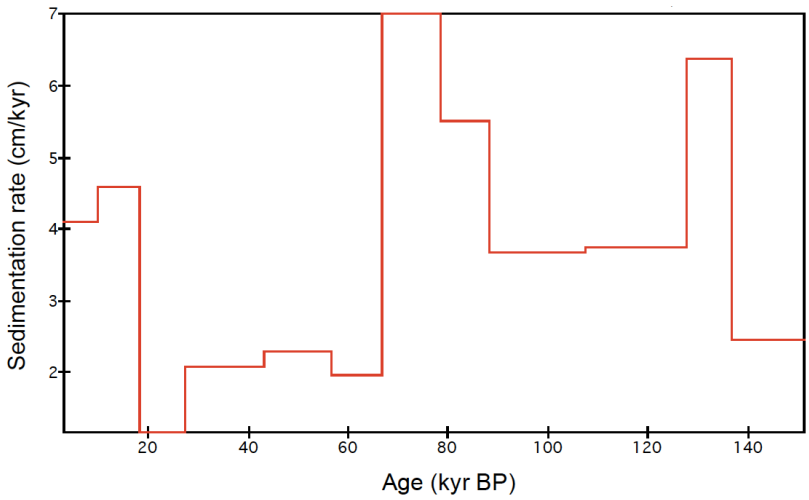

Fig. A.1: Sedimentation rate of core SO136-111.

B) Conventionally versus FTIRS-derived opal content

To assess the FTIRS-derived opal weight contents, 10 sediment samples were measured externally by alkaline extraction of biogenic silica at UBC, Vancouver, Canada. A high correlation between the different measurement techniques has been inferred with a correlation coefficient $R^2 = 0.90$ (see Fig. B.1). The residual deviation could be a consequence of internal measurement uncertainties and/or owing to minimal water adsorption after sample treatment, which interferes with the absorption spectra of biogenic silica in FTIRS analysis.

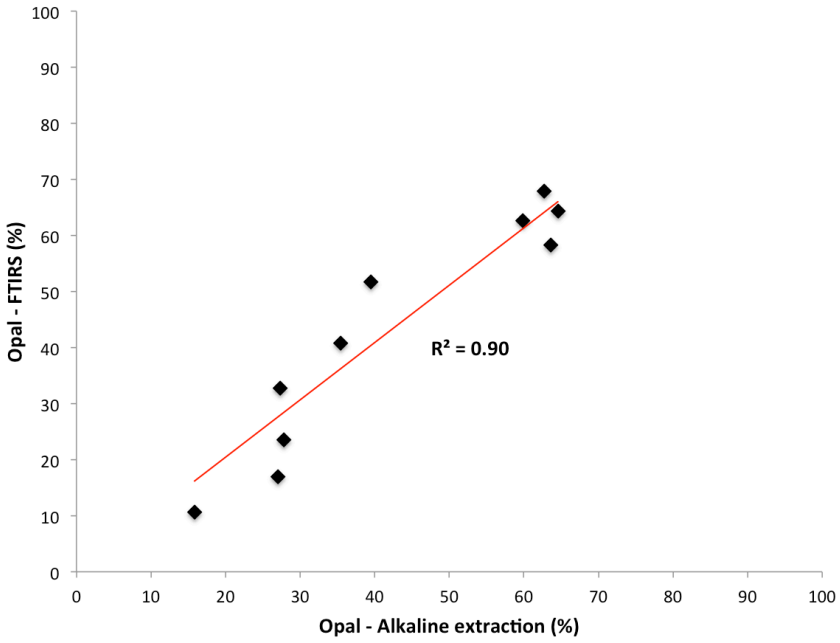

Fig. B.1. Correlation between conventionally and FTIRS-derived opal content.

C) U-Th calculation

To infer the activity of individual isotopes in the sediment, a spike solution with a known isotopic concentration was added to every sample. The calculation of the sedimentary isotopes is illustrated by the example of ^{232}Th with the aid of the ^{229}Th spike (Eq. C.1 and Eq. C.2).

$$\frac{229}{232} = \frac{c_{229} * m_{229}}{c_{232} * m_{232}} \qquad \text{(Eq. C.1)}$$

The ratio on the left hand side is the measured sample value, which is given by the weight (m) and concentration (c) of the respective isotopes. The concentration (pg/g) of the spike (c_{229}) is known, as well as the weight (mg) of the spike (m_{229}) and the sample (m_{232}), wherefore Eq. C.1 can be solved for c_{232}:

$$c_{232} = c_{229} * \frac{m_{229}}{m_{232}} * \frac{232}{229} * \theta * \varepsilon \qquad \text{(Eq. C.2)}$$

where ε is a conversion factor to calculate the activity in dpm/g out of pg/g. ε is different for every isotope, since it depends on the respective decay constant. The measured ratio (i.e. 229/232) deviates from the actual ratio in the sample due to measurement deviations, wherefore a machine-specific calibration constant θ is introduced to the final calculation. This constant includes the mass bias and more important the yield between different cups and ion counters. θ was calculated by the deviation of measured standards to the certified values from literature. By measuring blanks, additional corrections for spike contaminations were applied.

D) Data

A data table with all measurements from core SO136-111 is on the CD attached at the end.

11. Declaration

Declaration

under Art. 28 Para. 2 RSL 05

Last, first name: .....

Matriculation number: .....

Programme: .....

Bachelor ☐ Master ☐ Dissertation ☐

Thesis title: .....

.....

.....

Thesis supervisor: .....

.....

I hereby declare that this submission is my own work and that, to the best of my knowledge and belief, it contains no material previously published or written by another person, except where due acknowledgement has been made in the text. In accordance with academic rules and ethical conduct, I have fully cited and referenced all material and results that are not original to this work. I am well aware of the fact that, on the basis of Article 36 Paragraph 1 Letter o of the University Law of 5 September 1996, the Senate is entitled to deny the title awarded on the basis of this work if proven otherwise. I grant inspection of my thesis.

.....

Place, date

.....

Signature